Dynamics of T cell activation mediated by eIF3 interactions with T cell receptor mRNAs

Dasmanthie De Silva[1,2], Lucas Ferguson[1], Benjamin E. Smith[3], Grant H. Chin[1], Ryan A. Apathy[4], Theodore L. Roth[4], Marek Kudla[1], Alexander Marson[4,5,6,7,8,9], Nicholas T. Ingolia[1,10], Jamie H. D. Cate[1,2,9,11,12]*

1. Department of Molecular and Cell Biology, University of California-Berkeley, Berkeley, California 94720, United States.
2. The J. David Gladstone Institutes, San Francisco, CA 94158 USA
3. School of Optometry, University of California, Berkeley, Berkeley, CA 94720, USA.
4. Department of Microbiology and Immunology, University of California, San Francisco, San Francisco, CA, USA.
5. Diabetes Center, University of California, San Francisco, San Francisco, CA, USA.
6. Chan Zuckerberg Biohub, San Francisco, CA, USA
7. Department of Medicine, University of California, San Francisco, San Francisco, CA, USA.
8. Parker Institute for Cancer Immunotherapy, San Francisco, CA, USA.
9. Innovative Genomics Institute, University of California, Berkeley, Berkeley, CA, USA.
10. California Institute for Quantitative Biosciences, University of California, Berkeley, Berkeley, United States.
11. Department of Chemistry, University of California-Berkeley, Berkeley, California 94720, United States.
12. Molecular Biophysics and Integrated Bioimaging Division, Lawrence Berkeley National Laboratory, Berkeley, California 94720, United States.

* Corresponding author: jcate@lbl.gov

Abstract

Activation of T cells requires a global surge in cellular protein synthesis, which is accompanied by a large increase in translation initiation[1–4]. A central component of the translation initiation machinery–the multi-subunit eukaryotic initiation factor 3 (eIF3)–is rapidly turned on when quiescent T cells are stimulated[3]. However, the precise role eIF3 plays in activated T cells is not known. Using a global transcriptome cross-linking approach, we show that human eIF3 interacts with a distinct set of mRNAs in activated Jurkat cells. A subset of these mRNAs, including those encoding the T cell receptor (TCR) subunits TCRA and TCRB, crosslink to eIF3 across the entire length of the mRNA. Fluorescence in situ hybridization studies reveal both *TCRA* and *TCRB* mRNAs form granules, potentially acting as translation "hot-spots." We further find that elements in the 3'-untranslated regions (3'-UTRs) of the *TCRA* and *TCRB* mRNAs that directly interact with eIF3 control the early dynamics of TCR translation in a CD28-dependent manner, as well as the extent of T cell activation. These results highlight a new role for eIF3 in regulation of translation dynamics and provide insights that can guide engineering of T cells for cell immunotherapy applications.

Main

Several lines of evidence indicate eIF3 serves specialized roles in cellular translation, by recognizing specific RNA structures in the 5'-untranslated regions (5'-UTRs) of target mRNAs[5], binding the 7-methyl-guanosine (m^7G) cap[6] or through interactions with *N*-6-methyl-adenosine (m^6A) post-transcriptional modifications in mRNAs[7]. Binding to these *cis*-regulatory elements in mRNA can lead to translation activation or repression, depending on the RNA sequence and structural context[5–8]. These functions for eIF3 can aid cell proliferation[5], or allow cells to rapidly adapt to stress such as heat shock[7]. Additionally, eIF3 plays an important role in the development of specific tissues[9–11].

In the immune system, T cell activation involves a burst in translation[1–4] and correlates with assembly of subunit EIF3J with the main eIF3 complex[3]. However, whether eIF3 serves a general or more specific role in T cell activation is not known. To delineate how eIF3 contributes to T cell activation, we first identified mRNAs that directly interact with eIF3 in Jurkat cells activated for 5 hours with ionomycin and phorbol 12-myristate 13-acetate (I+PMA), or in non-activated Jurkat cells as a control, using photoactivatable ribonucleoside-enhanced crosslinking and immunoprecipitation (PAR-CLIP)[5,12,13] (**Fig. 1a**). We used Jurkat cells as a model for T cells, as PAR-CLIP experiments require a large number of cells labeled with 4-thiouridine at a non-toxic concentration[14]. Jurkat cells also have a defined T cell receptor and transcriptome, avoiding the donor-to-donor variability of primary T cells. In the Jurkat PAR-CLIP experiments, RNA crosslinked to eight of the thirteen eIF3 subunits, as identified by mass spectrometry: subunits EIF3A, EIF3B, EIF3D and EIF3G as seen in HEK293T cells[5], as well as subunits EIF3C,

EIF3E, EIF3F, and EIF3L (**Fig. 1b, Extended Data Fig. 1, Supplementary Table 1**). In activated Jurkat cells, eIF3 crosslinked to a substantially larger number of mRNAs compared to the non-activated cells (**Extended Data Figs. 2 and 3, Supplementary Tables 2 and 3**). Notably, eIF3 interacted with a completely new suite of mRNAs in activated Jurkat cells, compared to those identified in HEK293T cells (**Fig 1c, Extended Data Fig. 4, Supplementary Tables 4 and 5**). These mRNAs are enriched for those encoding proteins central to immune cell function (**Supplementary Table 6**). Moreover, eIF3 crosslinking does not correlate with mRNA abundance (**Extended Data Fig. 4**), suggesting that eIF3 is involved in specific regulation of T cell activation.

In activated Jurkat cells, eIF3 crosslinked to mRNAs by a multitude of patterns (**Fig 2a, b, Extended Data Fig. 5**), consistent with varied roles for eIF3 in T cell activation and function. Many of the mRNAs have a single PAR-CLIP site in the 5'-UTR as observed in HEK293T cells[5] (**Fig. 2a**, **Extended Data Figs. 2, Supplementary Table 6**). However, eIF3 crosslinked to some mRNAs across their entire length, from the beginning of the 5'-UTR through the 3'-UTR (**Fig. 2a, b, Extended Data Fig. 5**). This "pan-mRNA" pattern of eIF3 crosslinking–which includes polyadenylated mRNAs as well as histone mRNAs–has not been observed before. Notably, a number of these mRNAs encode proteins important for T cell activation, including both the alpha and beta subunits of the TCR, subunits TCRA and TCRB (**Fig. 2b**, **Supplementary Table 6**).

Crosslinking in PAR-CLIP experiments requires direct interaction between the RNA and protein of interest[14]. Thus, the pan-mRNA pattern of crosslinking between eIF3 and

certain mRNAs suggests formation of ribonucleoprotein complexes (RNPs) highly enriched in eIF3. Remarkably, the pan-mRNA crosslinking pattern in the *TCRA* and *TCRB* mRNAs occurs in activated but not non-activated Jurkat cells. As previously known RNPs such as processing bodies (P bodies) and stress granules contain translationally repressed mRNAs, we performed fluorescence in situ hybridization (FISH) on both *TCRA* and *TCRB* mRNAs in activated Jurkat cells. Since Jurkat cells have a defined TCR, we were able to design FISH probes across the entire *TCRA* and *TCRB* transcripts. We also probed for P body and stress granule proteins DCP1 and G3BP1, respectively[15–18]. Both the *TCRA* and *TCRB* mRNAs formed distinct puncta, but did not co-localize with either P bodies or stress granules, or with each other (**Fig. 2c, Extended Data Fig. 6**). Taken together, these results suggest that the *TCRA* and *TCRB* mRNA puncta represent eIF3-mRNA concentrated regions that may act as translation "hot spots."

Both the *TCRA* and *TCRB* mRNAs include prominent sites of eIF3 crosslinking in their respective 3'-UTR elements. To test the functional importance of these sites of eIF3 interaction, we used CRISPR-Cas9 genome editing with guide RNAs (gRNAs) targeted to the two boundaries of the eIF3 PAR-CLIP sites in each of the 3'-UTRs of *TCRA* and *TCRB* mRNA (**Extended Data Fig. 7, Supplementary Table 7**). We nucleofected these pairs of gRNA/Cas9 RNPs into primary human T cells from two donors, to delete the entire PAR-CLIP site in each 3'-UTR. PCR analysis showed successful deletion of the eIF3 PAR-CLIP site in the *TCRA* 3'-UTR or in the *TCRB* 3'-UTR (*TCRA* Δ*PAR* or *TCRB* Δ*PAR*, respectively) in approximately 50-60% of the cells (**Extended Data Fig. 7**). For

comparison with the *TCRA* Δ*PAR* or *TCRB* Δ*PAR* cell populations, we edited cells from both donors using each gRNA targeting the *TCRA* 3'-UTR and *TCRB* 3'-UTR region separately (single gRNA experiments), a gRNA targeting the coding sequence (CDS) of *TCRA* which knocks out TCR expression with high efficiency (Δ*TCR*)[19], a scrambled gRNA (SC) which does not target any site in the human genome, and cells mixed with the gRNA/Cas9 RNPs but not nucleofected.

We first measured total TCR protein levels in both the *TCRA* Δ*PAR* and *TCRB* Δ*PAR* cell populations by western blot, after different times following T cell stimulation using anti-CD3 and anti-CD28 antibodies (**Fig. 3a**). We used an anti-TCRA antibody to measure TCR levels in both *TCRA* Δ*PAR* and *TCRB* Δ*PAR* cells, since the formation of an intact TCR is required to stabilize both the TCRA and TCRB subunits[20,21]. In both *TCRA* Δ*PAR* and *TCRB* Δ*PAR* cell populations, TCRA protein levels were nearly absent or clearly reduced at early time points after activation (~1 hr). By contrast, SC control cells–which should behave as wild-type T cells–exhibited a substantial burst in TCRA protein levels immediately after activation (**Fig. 3a**). Only at later time points did TCRA levels in the *TCRA* Δ*PAR* and *TCRB* Δ*PAR* cell populations begin to increase. Next we checked whether the reduced TCR protein levels in *TCRA* Δ*PAR* and *TCRB* Δ*PAR* cell populations at early time points after activation with anti-CD3 and anti-CD28 antibodies affected the rate of TCR clustering, as occurs in immune synapse formation[22]. We used the same cell populations as those for western blot analysis (**Fig. 3a**), to correlate the TCRA protein levels observed in the western blots with TCR cluster formation. Using TCR protein staining, we observed a decrease in the proportion of

cells that formed TCR clusters in the *TCRA* Δ*PAR* and *TCRB* Δ*PAR* cell populations compared to SC control cells, with more severe defects seen at the earlier time points (**Fig. 3b**). We also stained cells with a fluorescently tagged anti-TCR antibody and used flow cytometric analysis to measure the levels of TCR on the cell surface with and without activation with I+PMA (**Fig. 3c, d, Extended Data Fig. 8**). A substantially lower percentage of the *TCRA* Δ*PAR* and *TCRB* Δ*PAR* cell populations expressed TCR on the cell surface compared to SC control cells or cells edited with a single gRNA (**Fig. 3c, d, Extended Data Fig. 8**). Taken together, these results suggest that regulation of TCR protein synthesis mediated by the *TCRA* and *TCRB* mRNA 3'-UTR elements that interact with eIF3 is required for the robust TCR clustering that is central to immune synapse formation[22].

To test whether the defect in TCR clustering in the *TCRA* Δ*PAR* and *TCRB* Δ*PAR* cell populations reflects a general deficiency in T cell activation, we measured the T cell activation markers CD69 and CD25 by flow cytometry and secreted cytokines IL2 and IFNγ using ELISA (**Fig. 4, Extended Data Figs. 9–12**). Both the CD4+ and CD8+ Δ*TCR* cell populations failed to express significant amounts of CD69 and CD25 (**Fig. 4a,b, Extended Data Fig. 10, Extended Data Fig. 11**), and the Δ*TCR* cells only weakly upregulated IL2 and IFNγ, particularly at the 24 hour time point (**Fig. 4c, Extended Data Fig. 12**). Notably, fewer cells in the *TCRA* Δ*PAR* and *TCRB* Δ*PAR* CD4+ and CD8+ cell populations expressed CD69 after 5 and 8 hours after activation, compared to SC control CD4+ and CD8+ cells (**Fig. 4a,b, Extended Data Fig. 10, Extended Data Fig. 11**). At later time points, fewer cells in the *TCRA* Δ*PAR* and *TCRB* Δ*PAR* cell

populations expressed both CD69 and CD25 activation markers compared to SC control cells. Furthermore, the *TCRA* Δ*PAR* and *TCRB* Δ*PAR* T cell populations secreted lower amounts of cytokines IL2 and IFNγ, compared to the SC control cells (**Fig. 4c, Extended Data Fig. 12**). Taken together, the *TCRA* Δ*PAR* and *TCRB* Δ*PAR* primary T cell populations exhibited activation defects at early and later time points, and align with the decreased TCR levels observed by western blot, detected by TCR clustering and by flow cytometry analyses (**Fig. 3**), consistent with eIF3-mediated regulation of T cell activation through interactions with the *TCRA* and *TCRB* mRNA 3'-UTR PAR-CLIP sites, in both CD4+ and CD8+ T cells.

To obtain a deeper mechanistic understanding of the role of eIF3 in the regulation of TCRA and TCRB translation, we recreated the deletions of the eIF3 PAR-CLIP sites in both the *TCRA* and *TCRB* mRNA 3'-UTRs (**Extended Data Fig. 7**) in Jurkat cells, which can be clonally propagated for detailed analysis. As observed in edited primary T cells, *TCRA* Δ*PAR* and *TCRB* Δ*PAR* Jurkat cell populations expressed lower levels of the TCR proteins compared to wild-type (WT) cells, and failed to show a burst in TCR expression at early time points after anti-CD3 and anti-CD28 activation (**Extended Data Fig. 13a**). Notably, *TCRA* and *TCRB* mRNA levels were unaffected or even increased in the *TCRA* Δ*PAR* and *TCRB* Δ*PAR* Jurkat cells (**Extended Data Fig. 13b, c**). Importantly, the amount of *TCRA* and *TCRB* mRNAs interacting with eIF3 was higher in WT cells than in the *TCRA* Δ*PAR* and *TCRB* Δ*PAR* cells after activation (**Extended Data Fig. 14**), indicating that deleting the eIF3 PAR-CLIP sites disrupts eIF3 interactions with these mRNAs. Additionally, the levels of eIF3-mRNA interaction closely

mirrored the total *TCRA* protein levels at both 5 hours and 8 hours for WT, *TCRA* Δ*PAR* and *TCRB* Δ*PAR* cells, suggesting that eIF3 interactions with the 3'-UTR sequences in the *TCRA* and *TCRB* mRNAs is tightly coupled with *TCRA* and *TCRB* protein levels. The *TCRA* Δ*PAR* and *TCRB* Δ*PAR* Jurkat cells also showed a delay in TCR clustering (**Extended Data Fig. 15**), had lower cell populations expressing CD69 and CD25, and secreted lower amounts of IL2 compared to WT cells (**Extended Data Fig. 16**), mirroring the results obtained in primary T cells (**Fig. 4, Extended Data Fig. 10-12**). These results verify that Jurkat cells recapitulate the response of primary T cells, and further support the model that eIF3 interactions with the PAR-CLIP sites in the *TCRA* and *TCRB* mRNA 3'-UTRs mediate translational regulation at early times after TCR activation.

In order to understand the functional role of eIF3 interactions with the 3'-UTRs of the *TCRA* and *TCRB* mRNAs, we constructed nanoluciferase reporters with the 5'-UTR of the human beta globin gene (*HBB*) and a PEST destabilization domain. The PEST domain reduces nanoluciferase protein half-life[23,24] and provides better time resolution of nanoluciferase expression after T cell activation. The reporter coding sequence (CDS) was then fused to the wild-type *TCRA* or *TCRB* mRNA 3'-UTR sequence (WT), or 3'-UTR with the eIF3 PAR-CLIP site deleted (*ΔPAR*), or 3'-UTR with the reversed sequence of the eIF3 PAR-CLIP site (R**PAR*, i.e. 5'-3' sequence reversed to 3'-5' direction) (**Fig. 5a**), and stably transduced into Jurkat cells using a lentiviral vector. Cells expressing nanoluciferase from reporters with a deletion or reversal of the eIF3 PAR-CLIP site sequence led to reduction of the luminescence signal compared to cells

expressing nanoluciferase with the WT 3'-UTR sequences (**Fig. 5b**). Furthermore, similar to the *TCRA* Δ*PAR* and *TCRB* Δ*PAR* Jurkat cell lines, there was no significant defect in the *TCRA* Δ*PAR* and *TCRA* R**PAR* nanoluciferase mRNA levels compared to intact *TCRA* 3'-UTR mRNA, or for *TCRB* Δ*PAR* and R**PAR* nanoluciferase mRNA levels compared to intact *TCRB* 3'-UTR mRNA through 5 hrs, when the biggest defect in luciferase translation is observed (**Extended Data Fig. 17a**)**.** Immunoprecipitation of eIF3 followed by qRT-PCR quantification of nanoluciferase mRNA showed that less nanoluciferase mRNA was bound to eIF3 when the 3'-UTR PAR-CLIP site was either deleted or reversed, compared to nanoluciferase mRNAs carrying the WT *TCRA* or *TCRB* 3'-UTR (**Fig. 5c**). These results support the model that eIF3 binding to the PAR-CLIP sites in the *TCRA* and *TCRB* mRNA 3'-UTRs is necessary for eIF3-mediated temporal regulation of TCRA and TCRB translation in activated T cells. We also tested the levels of nanoluciferase expression when the reporter was fused to other 3'-UTR sequences now in use for chimeric antigen receptor (CAR) expression in CAR-T cells in the clinic[25,26,27] and in next-generation CAR-T designs[28] (**Fig. 5d**). In contrast to the TCRA 3'-UTR, the other 3'-UTR elements failed to show a robust increase in nanoluciferase expression peaking 5 hr after activation (**Fig. 5d**, **Extended Data Fig. 17b**).

To identify which T-cell activation pathway[29] is responsible for the burst in TCRA protein levels observed immediately after activation, we stimulated primary T cells as well as Jurkat cells with anti-CD3 plus anti-CD28 antibodies combined, either anti-CD3 or anti-CD28 antibodies separately, or with PMA+IONO (**Fig. 6a** and **Extended Data Fig. 18a**).

The burst in TCRA protein levels occurred only when anti-CD28 antibody was present, even without anti-CD3 antibody, suggesting that the CD28 costimulatory pathway is crucial for the temporal regulation of TCR protein expression in both primary T cells as well as in Jurkat cells. To test the proximal signaling pathway downstream of CD28 required for dynamic regulation of TCR expression, we used three different small molecules to inhibit protein kinase AKT during activation using anti-CD3/anti-CD28 antibodies (**Fig. 6b,c** and **Extended Data Fig. 18b).** Notably, the AKT kinase-inhibited cells were unaffected at early time points relative to the untreated controls, but failed to show the temporal peak in TCR expression at 5-8 hours, suggesting that the TCR temporal expression pattern is regulated by AKT.

Recent experiments indicate that T cells must cross a “threshold” of T cell receptor signaling to commit to activation and proliferation[30,31], setting up a “digital” response to antigen recognition[30–33]. The response threshold involves integration of intensity and duration of TCR signaling[30,31,33], and spans a wide range of TCR antigen affinity[30–33]. Notably, T cell commitment to clonal expansion and differentiation can occur with as little as 1 to 2 hours of TCR stimulation for effector CD4+ and naive CD8+ T cells[34,35]. This time period spans the burst in TCR protein synthesis mediated by eIF3 interactions with the *TCRA* and *TCRB* 3’-UTR elements (**Fig. 3a**). Naive CD4+ T cells require a longer duration of TCR signaling of ~20 hours[34,36]. Although we were not able to distinguish levels of TCR translation in isolated CD8+ and CD4+ cells (**Fig. 3**), subsequent events in T cell activation including CD69 and CD25 expression, and IL2 and IFNγ secretion, were equally affected in CD8+ and CD4+ cells in which the 3’-UTR

PAR-CLIP sites were deleted (**Fig. 3, Fig. 4**). Importantly, we now show CD28-mediated signaling, which serves as the second signal required for T cell activation[37,38] and affects the first minutes of TCR-mediated signaling[39–43], is also needed for the dynamics of TCR translation on the hour timescale. Taken together, our results indicate eIF3 controls *TCRA* and *TCRB* mRNA translation during the first critical hours after TCR stimulation that lead to subsequent T cell commitment to proliferation and differentiation. Given that CD28 is required for PD-1 mediated inhibition of T cell activation[44,45], it will be interesting to determine the role of eIF3-mediated control of TCR expression in PD-1 checkpoint blockade-based cancer immunotherapy[46]. Additionally, our results suggest that eIF3-responsive mRNA 3'-UTR elements could be used to improve chimeric antigen receptor expression and CAR-T cell responsiveness[28,47].

The eIF3 PAR-CLIP experiment we present here provides a snapshot of eIF3-RNA interactions that occur at the time TCR translation is most sensitive to eIF3 regulation (5 hours in Jurkat cells, **Fig. 2b**, **Extended Data Fig. 13**). At this point in time, eIF3 crosslinks to multiple mRNAs encoding proteins involved in immune cell function (**Supplementary Table 6**). Interestingly, the patterns of eIF3 crosslinking, which for a number of mRNAs include interactions with the protein coding sequence and 3'-UTR (**Fig. 2**, **Extended Data Fig. 5b**), suggest an active role for eIF3 in promoting translation of these mRNAs. In support of this model, the two examples of pan-mRNAs we examined here (*TCRA* and *TCRB*) reside in puncta distinct from P bodies and stress granules (**Fig. 2c**). However, this eIF3-mediated translation activation is transient, lasting only 1-2 hours in primary T cells (**Fig. 3b**, **Extended Data Fig. 13a**). Recent

evidence suggests that eIF3 can remain associated with translating ribosomes[48,49,50], a phenomenon that may be enhanced for the pan-mRNAs identified here. Notably, additional layers of translation regulation also contribute to T cell function[51], particularly with respect to mTOR signaling[3,52] and carbon metabolism[4,53]. The present PAR-CLIP experiments should help to elucidate additional roles for eIF3-mediated translation regulation and to more fully map the system-wide role of translation regulation in T cell activation.

Figures

Figure 1. PAR-CLIP analysis of eIF3 interactions with RNAs in Jurkat cells. a, Schematic of Jurkat cell treatment with 4-thiouridine, activation, and cell harvesting for PAR-CLIP analysis. **b**, Phosphorimage of SDS polyacrylamide gel resolving 5′ ^{32}P-labeled RNAs crosslinked to eIF3 subunits in activated and non-activated Jurkat cells. **c**, Venn diagram of genes identified by eIF3 PAR-CLIP in the two biological replicates of activated Jurkat cells, compared with the eIF3 PAR-CLIP mRNAs identified in HEK293T cells. The same number of mRNAs from the Jurkat cell PAR-CLIP libraries, ranked by total reads mapped to a given gene, are compared to the number of mRNAs identified in the HEK293T PAR-CLIP experiments.

Figure 2. Varied mRNA crosslinking patterns to eIF3 in activated Jurkat cells. a, Cumulative plot showing mRNA crosslinking in sample EIF3A/C/B to predominantly the 5'-UTR (n = 396, 414 mRNAs in replicates 1 and 2, respectively), and across the entire length of some mRNAs (n = 634, 621 mRNAs). We defined mRNAs having a ratio of normalized 5'-UTR reads divided by 3'-UTR reads of 20 or more as "5'-UTR enriched" with respect to eIF3 crosslinking. All others were categorized as "pan-mRNAs," with eIF3 crosslinking across the entire length of the mRNA. The cut-off value 20 is not a sharp boundary between the two categories of mRNA (**Extended Data Fig. 5a**). The 5'-UTR, CDS, and 3'-UTR regions are shown normalized by length. **b**, Crosslinking of eIF3 subunits EIF3A/C/B, EIF3B/C and EIF3D/L across the entire *TCRA* and *TCRB* mRNAs. 5'-UTR, coding sequence (CDS), and 3'-UTR elements for the mapped TCR genes in

Jurkat cells are shown. Counts, PAR-CLIP reads from deep sequencing library analysis[54]. **c**, FISH analysis of *TCRA* and *TCRB* mRNAs (yellow and magenta, respectively) and P bodies (on the left) marked by the location of DCP1 (cyan) and stress granules (on the right) marked by the location of G3BP1 (cyan), in activated Jurkat cells. Graphs to the right of the images indicate Pearson's correlation coefficients (PCCs) of *TCRA* and *TCRB* mRNA with each other or with P bodies or stress granules. Labels on the x axis are, B: TetraSpeck™ microsphere beads, C: activated Jurkat cells. (n = 5, P <0.008, for PCC values of cells relative to bead colocalization, across all the channels tested, using the Wilcoxon rank-sum test). Images are representative of one experiment of the five independent experiments in the graphs.

Figure 3. TCR levels in activated primary human T cells with eIF3 3'-UTR PAR-CLIP sites deleted. a, Western blots measuring TCRA protein levels as a function of time after anti-CD3/anti-CD28 activation. Cell lines used are labeled on the left: *TCRA* Δ*PAR* (*TCRA* gRNA 1+2), *TCRB* Δ*PAR* (*TCRB* gRNA 1+2), and SC (scrambled gRNA). HSP90 was used as a loading control. Schematics of *TCRA* and *TCRB* mRNAs with and without eIF3 PAR-CLIP sites are shown above. SC control cells have the wild-type (WT) 3'-UTRs for *TCRA* and *TCRB* mRNAs. **b**, The number of T cells with one or more TCR clusters measured by anti-TCRA/anti-TCRB protein staining and epifluorescence microscopy as a function of time after anti-CD3/anti-CD28 activation. A total of 100 cells from each donor were imaged for *TCRA* Δ*PAR* (n = 2 donors, stained with anti-TCRA antibody), *TCRB* Δ*PAR* (n = 2 donors, stained with anti-TCRB antibody), and SC cell lines (n = 2 donors, each stained separately with anti-TCRA and anti-TCRB antibodies).

Values are mean ± standard deviation. P < 0.005 comparing *TCRA* Δ*PAR* and *TCRB* Δ*PAR* to SC after 1 hour of activation. P ≤ 0.0002 comparing *TCRA* Δ*PAR* and *TCRB* Δ*PAR* to SC after 3 hours of activation, using two-way ANOVA. **c**, Representative density plots showing the percentage of I+PMA activated T cells expressing TCR on the cell surface 3 hours after activation, measured by flow cytometric analysis for one of two donors. The cell lines shown are *TCRA* Δ*PAR*, *TCRB* Δ*PAR*, Δ*TCR* (negative control), and SC. **d**, Percent cells expressing TCR on the cell surface after I+PMA activation for 3 hours (*n* = *2* donors, with mean and standard deviation shown), reported in bar graph form. P < 0.0001 for *TCRA* Δ*PAR* or *TCRB* Δ*PAR* relative to SC, using one-way ANOVA.

Figure 4. Phenotypic analysis of primary human T cells. a, Flow cytometric analysis measuring T cell activation markers CD69 (early activation marker) and CD25 (mid-activation marker) in *TCRA* Δ*PAR*, *TCRB* Δ*PAR*, Δ*TCR* and SC CD8+ T cells, quantifying mean percent cells expressing CD69+ only (left) and CD69+ CD25+ (right) from (*n* = 2 donors). **b**, Density plots showing cell populations expressing CD69+ only, CD69+ CD25+ or CD25+ only from one of the donors. Cells sorted as shown in **Extended Data Fig. 9**. **c**, Quantification of secreted IL2 and IFNγ from cell lines *TCRA* Δ*PAR, TCRB* Δ*PAR,* Δ*TCR* and SC cell populations from (*n* = 2 donors) at different time points after stimulation with anti-CD3/anti-CD28 antibodies, as determined by ELISA. For both figures **a,** and **c,** Values are mean ± standard deviation, ****P < 0.0001 relative to SC, using two-way ANOVA. Differences in expression of activation markers

and secreted cytokines in comparisons of *TCRA* Δ*PAR* with *TCRB* Δ*PAR* were not significant.

Figure 5. Effects of *TCRA, TCRB*, and 3'-UTR variants on nanoluciferase reporter translation. a, Schematic of the nanoluciferase reporters stably expressed in Jurkat cells. WT, intact 3'-UTR from either *TCRA* or *TCRB* mRNA; *ΔPAR*, 3'-UTR of *TCRA* or *TCRB* with the eIF3 PAR-CLIP site deleted (nucleotides 102-338 in the 3'-UTR of *TCRA* mRNA or nucleotides 16-161 in the 3'-UTR of *TCRB* mRNA); R**PAR*, reversed PAR-CLIP sequence in the 3'-UTR of *TCRA* or *TCRB* mRNA. **b**, Luciferase activity in anti-CD3/anti-CD28 activated Jurkat cells, relative to non-activated controls (n = 3, with mean and standard deviations shown). $P < 0.0001$ for *TCRA* Δ*PAR* and R**PAR* relative to WT at 5 hr and 8 hr, and $P \leq 0.0002$ for 10 hr, using two-way ANOVA. $P < 0.0001$ for *TCRB* Δ*PAR* and R**PAR* relative to WT for 1 hr - 10 hr. **c**, Immunoprecipitation of eIF3 using an anti-EIF3B antibody[5], followed by qRT-PCR to quantify the amount of nanoluciferase mRNA bound to eIF3 (n = 3, with mean and standard deviations shown). The schematic of the experiment is indicated on the left. For *TCRA* and *TCRB* mRNAs, $P < 0.0001$ for Δ*PAR* and R**PAR* relative to WT, using two-way ANOVA. P values for IL2 mRNAs for Δ*PAR* and R**PAR* relative to WT were not significant. **d**, Luciferase activity from nanoluciferase reporters with either the intact 3'-UTR from *TCRA*, the Woodchuck Hepatitis Virus Posttranscriptional Regulatory Element (*WPRE*), the gammaretroviral 3'-Long Terminal Repeat (*3'-LTR*), or bovine growth hormone polyadenylation signal (*bpA*) following the nanoluciferase coding sequence, as shown in the schematic (n = 3, with mean and standard deviations shown). $P < 0.03$ for *WPRE*

and *bpA* relative to *TCRA* 3'-UTR at 1 h. $P < 0.0001$ for *WPRE*, *3'-LTR* and *bpA* relative to *TCRA* 3'-UTR for 2 hr -10 hr, using two-way ANOVA.

Figure 6. Regulatory pathways leading to dynamics of TCR protein expression levels. a, Western blots of TCRA protein levels in primary human T cells using different activation modes. **b,** Western blot of TCRA protein levels in Jurkat cells activated with anti-CD3/anti-CD28 antibodies. An anti-Phospho-GSK-3β antibody was used to measure AKT activity. **c,** Western blot of TCRA protein levels in Jurkat cells activated with anti-CD3/anti-CD28 antibodies in the presence of AKT inhibitor AZD5363. In all panels HSP90 was used as a loading control. Experiments with AKT inhibitors were carried out in duplicate.

Materials and methods

Jurkat cell culture

Human Jurkat, Clone E6-1 (ATCC TIB-152) was purchased from American Type Culture Collection (ATCC) and was maintained in RPMI 1640 Medium (ATCC modification) with 10% FBS (VWR Life Science Seradigm) and 0.01% Penicillin-Streptomycin (10,000 U/mL). The cells were maintained between 1 million to 8 million cells/mL. When cells were stimulated they were always maintained at 8 million cells/mL.

Isolation of human primary T cells

Primary human T cells were isolated from healthy human donors from leukoreduction chambers after Trima Apheresis (Vitalant, formerly Blood Centers of the Pacific). Peripheral blood mononuclear cells (PBMCs) were isolated from whole blood samples by Ficoll centrifugation using SepMate tubes (STEMCELL) per manufacturer's instructions. T cells were isolated from PBMCs from all cell sources by magnetic negative selection using an EasySep Human T Cell Isolation Kit (STEMCELL), per manufacturer's instructions. Unless otherwise noted, isolated T cells were stimulated as described below and used immediately.

Primary human T cell culture

Bulk T cells were cultured in XVivo15 medium (STEMCELL) with 5% fetal bovine serum (FBS), 50 μM 2-mercaptoethanol, and 10 μM *N*-acetyl-cystine. Immediately after isolation, T cells were stimulated for 2 days with anti-human CD3/CD28 magnetic

Dynabeads (ThermoFisher) at a bead to cell concentration of 1:1, along with cytokine IL-2 at 500 U/mL (UCSF Pharmacy). After electroporation, T cells were cultured in media with IL-2 at 500 U/mL. Throughout the culture period T cells were maintained at an approximate density of 1 million cells per mL of media. Every 2–3 days after electroporation, additional media was added, along with additional fresh IL-2 to bring the final concentration to 500 U/mL, and the cells were transferred to larger culture flasks as necessary to maintain a density of 1 million cells per mL.

For the T cell stimulation assay, edited primary T cells were transferred to fresh media lacking IL2 after 9 days of culturing. The T cells were then stimulated with anti-CD3 and anti-CD28 antibodies using flat bottom plates coated with anti-CD3 antibody (at a 10 µg/mL concentration), and anti-CD28 antibody added to the cell culture media at a concentration of 5 µg/mL.

Jurkat cell stimulation

The Jurkat cells used for the for the PAR-CLIP experiment were stimulated with 1X Cell Stimulation Cocktail, containing phorbol 12-myristate 13-acetate (PMA) and ionomycin (Thermofisher, Catalog number: 00-4970-93). Unless otherwise stated all other Jurkat cell simulations were performed with anti-CD3 and anti-CD28 antibodies (Tonbo). Flat bottom plates were coated with anti-CD3 antibody (at a 10 µg/mL concentration), and anti-CD28 antibody was added to the cell culture media at a concentration of 5 µg/mL.

Treatment of Jurkat cells with AKT inhibitors

Jurkat cells were treated with either MK-2206 at 3 µM (Cayman Chemical), AZD5363 at 1 µM (Cayman Chemical), GSK690693 at 2 µM (Cayman Chemical) or DMSO (control) for 3 hours prior to activation with anti-CD3 and anti-CD28 antibodies (Tonbo) as described above. The cells were collected at the indicated time points and processed for western blot analysis[55].

4-thiouridine optimization

Jurkat cells were seeded, so that they reached $8X10^5$ cells ml^{-1} seeding density on the day of the experiment. Varying concentrations of s4U were added to the cells (50 uM, 75 uM, 100 uM, or none as a negative control). The cells were then incubated for different time points: 8 hours, 10 hours, 12 hours, or 16 hours. After each incubation time cell viability was determined using the CellTiter-Glo assay (Promega), according to the manufacturer's instructions. Concentrations at which the relative luminescence in the presence of s4U (luminescence of the s4U treated cells/luminescence of the untreated cells) exceeded 95% were considered non-toxic. Based on these measurements, we used 50 µM of 4-thiouridine for PAR-CLIP experiments.

PAR-CLIP

Two biological replicates were used to perform PAR-CLIP analysis as described in[5], with modifications for Jurkat cells. 50 µM of 4-thiouridine was determined as non toxic to

Jurkat cells over the time course of the PAR-CLIP experiments[14]. A total of 55 million Jurkat cells seeded at 8 million cells ml^{-1} was treated with 50 µM of 4-thiouridine (Sigma) for 7 hours, then stimulated with 1X Cell Stimulation Cocktail for 5 hours in media containing 50 µM of 4-thiouridine (**Fig. 1a**). The same number of cells were treated with 50 µM of 4-thiouridine (Sigma) for 12 hours without stimulation as a non-activated control. The cells were then crosslinked on ice with 365 nm UV irradiation at an energy dose of 0.2 J cm^{-2}. The cells were pelleted by centrifugation at 100 x g for 15 min at 4 °C, and the pellet was resuspended in three volumes of NP40 lysis buffer (50 mM HEPES-KOH pH 7.5, 150 mM KCl, 2 mM EDTA, 0.5% Nonidet P-40 alternative, 0.5 mM dithiothreitol (DTT), 1 Complete Mini EDTA-free Protease Inhibitor Cocktail tablet (Roche)). The cell suspension was then incubated on ice for 10 min, passed through an 18G needle five times, and centrifuged at 13,000 x g for 15 min at 4 °C and RNAs were lightly digested by treatment with MNase (Thermo Scientific) at a final concentration of 0.05 U $µl^{-1}$ for 20 min at 16 °C. For each PAR-CLIP assay 1000 µl of Dynabeads (Invitrogen) and 800 µl of anti-EIF3B antibody (Bethyl A301-761A) were used. The remaining steps of the PAR-CLIP analysis was performed exactly as described in [5,56] with the exception of using MNase at 5 U $µl^{-1}$ for the on-bead digestion step.

PAR-CLIP computational analysis

PAR-CLIP cDNA libraries were sequenced on an Illumina HiSeq 2500 platform. To eliminate potential PCR biases during PAR-CLIP library preparation, a random bar code was introduced into the 3' adapter and all the reads that matched the random barcode were collapsed into single reads. Clusters of overlapping sequence reads mapped against the human genome version hg38 were generated using the PARalyzer

software[54] incorporated into the PARpipe pipeline (https://ohlerlab.mdc-berlin.de/software/PARpipe_119/, [13]) with the settings below. Binding sites were categorized using the Gencode GRCh38.p12 GTF annotations (gencode.v21.annotation.gtf), https://www.gencodegenes.org/human/.

The PARpipe settings used were:

Conversion = T>C

Minimum read count per group = 5

Minimum read count per cluster = 7

Minimum read count for kde = 3

Minimum cluster size = 11

Minimum conversion locations for cluster = 2

Minimum conversion count for cluster = 2

Minimum read count for cluster inclusion = 1

Minimum read length = 20

Maximum number of non conversion mismatches = 1

Comparison of eIF3 PAR-CLIP results in Jurkat and HEK293T cells

To compare RNAs in activated Jurkat cells crosslinked to eIF3 with those crosslinked to eIF3 in HEK293T cells[5], the gene cluster lists (*.gene_cl.csv) from APA_REP1, APA_REP2, APB_REP1, APB_REP2, APD_REP1, and APD_REP2 were used (see **Supplementary Table 3**). The genes were first sorted by total read counts ("ReadCountSum") from high to low for each library to obtain the top candidate genes.

Then, the same number of top candidate genes from these sorted lists as the number of genes identified in HEK293T cells, for eIF3 subunit EIF3A, EIF3B, and EIF3D crosslinked to RNA[5], were chosen for comparison.

PAR-CLIP Pathway analysis

To determine biological pathways enriched in the set of mRNAs that crosslinked to eIF3 in activated Jurkat cells, genes with at least 100 total aligned reads were used, as determined in the PARpipe analysis described above[13], from the EIF3A/C/B samples. Since PAR-CLIP reads are short, it is not possible to determine with certainty which mRNA transcript isoform cross-linked with eIF3. Therefore the most abundant mRNA transcript isoform for each gene was chosen, as determined by transcriptome profiling using kallisto (protein_coding category)[57], as described in the Transcriptome Profiling section. Even with this choice, eIF3 crosslinks to mRNAs do not correlate with mRNA abundance (**Extended Data Figure 4b**). Human genome GRCh38.p13 annotation was used to extract mRNA lengths by 5'-UTR, coding region and 3'-UTR (Ensembl Biomart)[58]. These genes were then sorted by the density of PAR-CLIP reads in the mRNA 5'-UTR region, prior to mapping pathways of transcripts that cross-linked to eIF3. Due to the complexity of *TCRA* and *TCRB* transcript annotation, these transcripts were excluded from the normalization calculation, but included in the pathway analysis. The top 500 genes from the resulting EIF3A/C/B PAR-CLIP gene lists were used, sorted as described above, to analyze gene enrichment profiles in the STRING database[59]. The top tissue-specific categories involve the immune system and T cell function

(**Supplementary Table 6**). Note that the STRING database does not include TCR subunits in its analysis.

Metagene analysis

The PAR-CLIP genes sorted as described above in the "PAR-CLIP pathway analysis" were used and mapped against the most abundant mRNA transcript isoforms to generate cumulative plots of the reads. Reads for the *TCRA* and *TCRB* mRNAs were manually extracted from the Bowtie version 1.0.0 Hg38 alignment of the eIF3 PAR-CLIP reads. We did not identify reads mapped to the D segment of *TCRB* (ie to *TRBD2*) due to its short length of 16 nucleotides. These reads were combined with the mapped reads in the *.read.csv files generated by Parpipe. The combined reads were then sorted to extract only reads annotated as 5'-UTR, start codon, coding, stop codon, and 3'-UTR. The most abundant transcript isoform, as identified in the transcriptome profiling using kallisto (described below) was used. Reads mapped to the 5'-UTR and start codon were normalized by the length of the 5'-UTR. Reads mapped to the coding region and stop codon were normalized by the length of the coding region. Finally, reads mapped to the 3'-UTR were normalized to the length of the 3'-UTR. Relative positions of the mapped reads along a metagene were computed based on the locations each mapped read fell within its respective feature. Relative positions were from -1 to 0 for the 5'-UTR, 0 to 1 for the coding region, and 1 to 2 for the 3'-UTR. 5'-UTR values were computed by multiplying the relative position by -1, whereas the 3-UTR values were were computed by adding 1 to the relative position. Coding region relative positions were unchanged.

The empirical cumulative distribution frequency function from R package ggplot2[60] was used to build the metagene plots from the vector of relative positions for the reads which mapped to a given set of reads.

We defined mRNAs having a ratio of normalized 5'-UTR reads divided by 3'-UTR reads of 20 or more as 5'-UTR enriched with respect to eIF3 crosslinking. All others were categorized as mRNAs with eIF3 crosslinking across the entire length of the mRNA. The cut-off value 20 is not a sharp boundary between the two categories of mRNA (**Extended Data Fig. 5a**).

Transcriptome Profiling

RNA samples were extracted from HEK293T cells, non-activated Jurkat cells, and Jurkat cells activated for 5 hr with I+PMA, using the Direct-zol RNA Miniprep kit (Zymoresearch). The libraries were prepared using TruSeq Stranded RNA LT Ribo-Zero Gold kit (Illumina) following the manufacturer's instructions, with two biological replicates per condition. Cutadapt (version 2.6)[61] with a minimum read length of 20, 5' end with a cutoff of 15 and the 3' end with a cutoff of 10 in paired-end mode was used to remove adapters. RNA-seq reads were pseudoaligned using kallisto v.0.46.0 run in quant mode with default parameters to estimate transcript abundance (transcripts per million, TPM)[57]. The transcript index for kallisto was made with default parameters and GENCODE Release 32 (GRCh38.p13) FASTA file[62].

To compare HEK293T or non-activated Jurkat mRNA abundance with that in activated Jurkat cells, the output from kallisto was used for analysis using DeSeq2 (ref [63]). All protein-coding transcripts (protein_coding) were then selected for the comparisons, using tximport[64] as part of the Bioconductor environment in R. All genes with ≥ 50 reads summed across all four samples in a comparison (two biological replicates per condition) were then used. Prior to making MA plots, the Approximate Posterior Estimation for generalized linear model (apeglm) shrinkage estimator for log fold changes was used[65] DeSeq2 output in **Supplementary Table 5** is presented prior to shrinkage analysis.

Mass spectrometry

To identify eIF3 subunits that crosslinked with RNAs in the PAR-CLIP experiments, a portion of eIF3 immunoprecipitated using Dynabeads as described above were treated with nonradioactive ATP during the T4 PNK labeling step. The nonradioactive samples were then run on the same gel next to the radiolabeled PAR-CLIP samples, Coomassie stained (Pierce) and the bands that matched with the phosphorimager printout were excised from the gel and submitted for identification using one-dimensional LC-MS/MS (**Supplementary Table 1**).

sgRNA/Cas9 RNP production

The sgRNA/Cas9 RNPs used to edit Jurkat cells were produced by complexing sgRNA (Synthego) to Cas9 as described[66] while RNPs to edit Primary Human T cells were

produced by complexing a two-component gRNA (crRNA and tracrRNA, Dharmacon) to Cas9 as described in[19]. The targeting sequences for the sgRNAs and crRNA are given in **Supplementary Table 7**. Recombinant Cas9-NLS was obtained from MacroLab in the California Institute for Quantitative Biosciences.

Jurkat and primary T cell genome editing

Jurkat cells used for electroporation were collected at passage 5 or lower and were maintained at a seeding density of 8 million cells ml^{-1} or lower. Primary T cells were isolated as described above. Prior to electroporation the Primary T cells were stimulated with magnetic anti-CD3/anti-CD28 Dynabeads (ThermoFisher) for 48 hours. After 48 hours these beads were removed from the cells by placing cells on an EasySep cell separation magnet for 2 min before electroporation. One million Jurkat (not activated) or primary T cells cells (activated with anti-CD3/anti-CD28 Dynabeads for 48 hours) were rinsed with PBS and then resuspended in 20 µl of Lonza electroporation buffer P3. The cells were then mixed with 2.5 µl Cas9 RNPs (50 pmol total) along with 2 µl of a 127-nucleotide non-specific single-stranded DNA oligonucleotide at 2 µg $µl^{-1}$ (4 µg ssDNA oligonucleotide total). The cells were then electroporated per well using a Lonza 4D 96-well electroporation system with pulse code DN100 for Jurkat cells and EH115 for primary human T cells. Immediately after electroporation, 80 µl of pre-warmed media (without cytokines) was added to each well, and the cells were allowed to rest for 15 min at 37 °C in a cell culture incubator while remaining in electroporation cuvettes. After 15 min, cells were moved to final culture flasks.

Western Blot

Western blot analysis was performed using the following antibodies: anti-TCRA (SC-515719), anti-HSP90 (SC-69703) (**Supplementary Table 7**).

Total mRNA isolation and quantitative RT-PCR analysis

Total RNA was isolated from whole cells for qRT-PCR using Quick RNA miniprep plus kit from Zymo Research following the manufacturer's instructions. Quantitative RT-PCR analysis was performed using the Power SYBR Green RNA-to-Ct 1-Step kit (Applied Biosystems) according to the manufacturer's instructions, and the QuantStudio™ 3 Real-Time PCR System (ThermoFisher). Each target mRNA was quantified in three biological replicates, with each biological replicate having three technical replicates.

Plasmids

The *TCRA* 3'-UTR and *TCRB* 3'-UTR sequences were amplified from Jurkat genomic DNA. The nanoluciferease sequence fused to a PEST domain was amplified from pNL1.2[*NlucP*] Vector Sequence (Promega) and was cloned into a modified CD813A vector (System Biosciences) containing the beta-globin (*HBB*) 5'-UTR using the In-Fusion® HD Cloning Kit (Takara). The subsequent mutations in the *TCRA* and *TCRB* 3'-UTRs were generated using these initial constructs. *TCRA/TCRB* Δ*PAR, R*PAR, 3'-LTR* (3'-Long Terminal Repeat) and *bpA* (bovine growth hormone polyadenylation signal) sequences were purchased as gblocks from IDT and were cloned into this plasmid backbone.

Generation of stable Jurkat cell lines expressing nanoluciferase reporter

For lentiviral production HEK293T cells were plated at a density of 80% in T-75 flasks the night before transfection. The cells were then transfected with plasmids: expressing the nanoluciferase, PsPAX2 and pCMV-VSV-G using the Lipofectamine 3000 reagent (ThermoFisher) following the manufacturer's instructions. Forty-eight hours after transfection, the viral supernatant was collected, filtered and concentrated using PEG-it Virus Precipitation Solution (System Biosciences) following the manufacturer's instructions. The virus pellets were then resuspended in RPMI-1640 media and stored in -80°C.

The Jurkat cell transductions were done with multiple viral titers using TransDux™ MAX Lentivirus Transduction Reagent (System Biosciences) following the manufacturer's instructions. To test the viral transduction efficiency of the cells, forty-eight hours after viral transduction the percent of cells expressing GFP was measured by FACS analysis and cells expressing less than 15% GFP were treated with 1µg ml^{-1} puromycin to the media. The cells were maintained in media with 1µg ml^{-1} puromycin, but transferred into media without puromycin the day before the cells were used for assays.

Luciferase reporter assay

The stable cell lines expressing the Nanoluciferease reporter were stimulated with anti-CD3 and anti-CD28 antibodies and the nanoluciferase activity was assayed after 1 hr, 3 hr, 5 hr, 8 hr, 10 hr and 24 hrs after stimulation using Nano-Glo® Luciferase Assay

System (Promega). For each time point 200,000 cells were tested in triplicate for each cell line.

RNA immunoprecipitation and qPCR

The EIF3B-RNA immunoprecipitations were carried out following the exact same conditions used for the PAR-CLIP analysis with the following changes. For each immunoprecipitation, cell lysates were prepared in NP40 lysis buffer (50 mM HEPES-KOH pH 7.5, 150 mM KCl, 2 mM EDTA, 0.5% Nonidet P-40 alternative, 0.5 mM DTT, 1 Complete EDTA-free Proteinase Inhibitor Cocktail tablet per 50 ml of buffer) with 4 million cells. The lysates were then incubated with 50 µl Protein G Dynabeads conjugated with 20 µl of anti-EIF3B antibody (Bethyl A301-761A) for two hours at 4 °C. After incubation, the flow through was removed and the beads were washed three times with 1 ml NP40 lysis buffer for each wash. The beads were then resuspended in 400 µl TRIzol reagent (ThermoFisher) and vortexed for 1 minute. The RNA was extracted following the manufacturer's instructions and qPCR was performed as described above using primers listed in **Supplementary Table 7**.

Flow cytometry and cell sorting.

Flow cytometric analysis was performed on an Attune NxT Acoustic Focusing Cytometer (ThermoFisher). Surface staining for flow cytometry and cell sorting was performed by pelleting cells and resuspending in 50 µl of FACS buffer (2% FBS in PBS) with antibodies at the indicated concentrations (**Supplementary Table 7**) for 20 min at 4 °C in the dark. Cells were washed twice in FACS buffer before resuspension.

ELISA

The cell suspensions were collected after each time point of activation with anti-CD3/anti-CD28 antibodies for WT, *TCRA* Δ*PAR* or *TCRB* Δ*PAR* cells. For each timepoint the same number of cells were used from each strain to be able to compare across strains and time points. The amount of secreted IL2 in the cell suspensions after activation anti-CD3/anti-CD28 antibodies for WT, *TCRA* Δ*PAR* or *TCRB* Δ*PAR* cells were measured by ELISA MAX™ Deluxe Set Human IL-2 (BioLegend) according to the manufacturer's instructions.

RNA-FISH and immunofluorescence

Jurkat cells were washed with PBS, fixed with 3.7% (vol./vol.) formaldehyde for 10 min at room temperature and washed three times with PBS. PBS was discarded and 1 ml 70% ethanol was added. The cells were incubated at 4 °C for 16 hours. The 70% ethanol was aspirated and the cells were washed once with 0.5 ml Stellaris RNA wash buffer A (Biosearch technologies). The cells were then incubated with 100 µl Stellaris hybridization buffer (Biosearch Technologies) containing Stellaris RNA FISH probes (Biosearch Technologies) at a final concentration of 125 nM (**Supplementary Table 7)** and with the relevant antibody (**Supplementary Table 7)** for 16 hours at 28 °C. The cells were then washed twice with 0.5 ml Stellaris RNA wash buffer A containing secondary antibody conjugated with a fluorophore for 30 minutes at 37 °C in the dark. The second Stellaris RNA wash buffer A contained DAPI in addition to the secondary antibody. Finally the cells were washed once with 0.5 mL Stellaris RNA wash buffer B and mounted with mounting solution (Invitrogen). All high resolution images were taken

using confocal ZEISS LSM 880 in Airyscan super-resolution mode, equipped withA Plan-Apochromat 63x/1.4 Oil objective (Zeiss). To measure colocalization of *TCRA* and *TCRB* mRNAs with each other or with P bodies (using DCP1 antibody) or stress granules (G3BP1 antibody) the cells were mounted along with 0.1 µm TetraSpeck™ microspheres (ThermoFisher) adhered to the slide according to manufacturer's instructions, to be able to account for the chromatic shift during image acquisition. For the counting of cells containing TCR clusters, a Revolve Epi-Fluorescence microscope (Echo), equipped with an A Plan-Apochromat 40x objective (Olympus) was used.

Colocalization analysis

To measure colocalization of *TCRA* and *TCRB* mRNAs with each other or with P bodies (using DCP1 antibody) or stress granules (G3BP1 antibody), immunofluorescently labelled cells (see above) were mounted along with 0.1 µm TetraSpeck™ microspheres (ThermoFisher) adhered to the slide according to manufacturer's instructions, to be able to account for the lateral and axial chromatic aberrations during image acquisition.

Z-stacks were acquired with 35 nm x 35 nm x 190 nm voxels on a ZEISS LSM 880 in Airyscan super-resolution mode, equipped with a Plan-Apochromat 63x/1.4 Oil objective (Zeiss). The images were then deconvolved to a lateral resolution of ≈150 nm and an axial resolution of ≈500 nm (as confirmed by observing the discrete Fourier transform of the z-stacks). After imaging a single cell, beads that were on the slide axial to the cell were imaged to measure the corresponding lateral and axial chromatic aberrations.

To quantify the relative colocalization, we developed an automated processing and analysis pipeline in ImageJ 1.52p available on github: https://github.com/Llamero/TCR_colocalization_analysis-macro. Specifically, the chromatic aberrations in the z-stacks were compensated for by registering the channels of the bead z-stack to one another, and then applying the same registration vectors to the corresponding channels in the cell z-stack[67]. Each channel of a z-stack was then thresholded to remove background in the image, and then the colocalization between each pair of images was measured using the Pearson's correlation coefficient. Samples in which any pair of channels in the bead z-stack had a correlation of less than 0.45 were removed from final analysis, as this suggested that the images had insufficient dynamic range in at least one of the channels for an accurate deconvolution.

Data and Code Availability

Sequencing data supporting the findings in this study have been deposited in the Gene Expression Omnibus (GEO) Database (https://www.ncbi.nlm.nih.gov/geo/), with accession codes _____. Code used to analyze the microscopy images is available on github at https://github.com/Llamero/TCR_colocalization_analysis-macro. Raw data for **Figure 3a**, **Extended Data Figure 1b**, and **Extended Data Figure 13a** are provided in Supplementary Figures 1-3.

Acknowledgements

We thank M. Hafner for advice on PAR-CLIP methodology and data analysis, A. Weiss for experimental suggestions and advice, H. Nolla and A. Valeros at the UC Berkeley

flow cytometry facility for helping out with the FACS analysis and single cell sorting, F. Ives and H. L. Aaron at the UC Berkeley Imaging center for help with microscopy, J. Lui for advice on planning experiments and for suggestions on the manuscript, and M. Mignardi for advice on FISH experiments. This work was supported by NIH grant R01-GM065050 (J.H.D.C.) and a grant from the Tang Prize for Biopharmaceutical Science (J.H.D.C.). N.T.I. is a Damon Runyon-Rachleff Innovator (DRR#37-15) and NIH New Innovator (DP2 CA195768). A.M. holds a Career Award for Medical Scientists from the Burroughs Wellcome Fund and The Cancer Research Institute (CRI) Lloyd J. Old STAR grantand has received funding from the Chan Zuckerberg Biohub, Innovative Genomics Institute (IGI) and the Parker Institute for Cancer Immunotherapy (PICI). B.E.S. is supported by NIH grant P30EY003176. Imaging experiments were conducted at the Cancer Research Laboratory Molecular Imaging Center, supported by Helen Wills Neuroscience Institute. Sequencing was carried out at the UCSF Center for Advanced Technology and at the Vincent J. Coates Genomics Sequencing Laboratory at UC Berkeley, supported by NIH grant S10 OD018174.

Author Contributions

Project and experiments were conceived and designed by D.D.S. and J.H.D.C. D.D.S. carried out all experiments, with assistance from B.E.S. and G.H.C. for image acquisition and analysis, from T.R., R.A.A., and A.M. for primary T cell genome editing and cell culture protocols, and from L.F., M.K., N.T.I. and J.H.D.C. for analysis of the deep sequencing-based experiments. The manuscript was written by D.D.S. and J.H.D.C., with editing by all authors.

Competing Interests

The authors declare competing financial interests: T.L.R. and A.M. are co-founders of Arsenal Therapeutics. A.M. is a co-founder of Spotlight Therapeutics. A.M. served on the scientific advisory board of PACT Pharma, was an advisor to Juno Therapeutics and Trizell. The Marson Laboratory has received sponsored research support from Juno Therapeutics, Epinomics, Sanofi and a gift from Gilead and Anthem. A provisional patent application has been filed on some of the work presented herein.

Materials and Correspondence

Correspondence and requests for materials should be addressed to J.H.D.C., jcate@lbl.gov.

Bibliography

1. Ahern, T., Sampson, J. & Kay, J. E. Initiation of protein synthesis during lymphocyte stimulation. *Nature* **248**, 519–521 (1974).
2. Kleijn, M. & Proud, C. G. The regulation of protein synthesis and translation factors by CD3 and CD28 in human primary T lymphocytes. *BMC Biochem.* **3**, 11 (2002).
3. Miyamoto, S., Patel, P. & Hershey, J. W. B. Changes in ribosomal binding activity of eIF3 correlate with increased translation rates during activation of T lymphocytes. *J. Biol. Chem.* **280**, 28251–28264 (2005).
4. Ricciardi, S. *et al.* The Translational Machinery of Human CD4+ T Cells Is Poised for Activation and Controls the Switch from Quiescence to Metabolic Remodeling. *Cell Metab.* **28**, 895–906.e5 (2018).
5. Lee, A. S. Y., Kranzusch, P. J. & Cate, J. H. D. eIF3 targets cell-proliferation messenger RNAs for translational activation or repression. *Nature* **522**, 111–114 (2015).
6. Lee, A. S., Kranzusch, P. J., Doudna, J. A. & Cate, J. H. D. eIF3d is an mRNA cap-binding protein that is required for specialized translation initiation. *Nature* **536**, 96–99 (2016).
7. Meyer, K. D. *et al.* 5’ UTR m(6)A Promotes Cap-Independent Translation. *Cell* **163**, 999–1010 (2015).
8. de la Parra, C. *et al.* A widespread alternate form of cap-dependent mRNA translation initiation. *Nat. Commun.* **9**, 3068 (2018).
9. Curran, S. P. & Ruvkun, G. Lifespan regulation by evolutionarily conserved genes essential for viability. *PLoS Genet.* **3**, e56 (2007).

10. Choudhuri, A., Maitra, U. & Evans, T. Translation initiation factor eIF3h targets specific transcripts to polysomes during embryogenesis. *Proc. Natl. Acad. Sci. U. S. A.* **110**, 9818–9823 (2013).
11. Cattie, D. J. *et al.* Mutations in Nonessential eIF3k and eIF3l Genes Confer Lifespan Extension and Enhanced Resistance to ER Stress in Caenorhabditis elegans. *PLoS Genet.* **12**, e1006326 (2016).
12. Hafner, M. *et al.* Transcriptome-wide identification of RNA-binding protein and microRNA target sites by PAR-CLIP. *Cell* **141**, 129–141 (2010).
13. Mukherjee, N. *et al.* Deciphering human ribonucleoprotein regulatory networks. *Nucleic Acids Res.* **47**, 570–581 (2019).
14. Ascano, M., Hafner, M., Cekan, P., Gerstberger, S. & Tuschl, T. Identification of RNA-protein interaction networks using PAR-CLIP. *Wiley Interdiscip. Rev. RNA* **3**, 159–177 (2012).
15. Hubstenberger, A. *et al.* P-Body Purification Reveals the Condensation of Repressed mRNA Regulons. *Mol. Cell* **68**, 144–157.e5 (2017).
16. Aizer, A. *et al.* Quantifying mRNA targeting to P-bodies in living human cells reveals their dual role in mRNA decay and storage. *J. Cell Sci.* **127**, 4443–4456 (2014).
17. Aulas, A. *et al.* G3BP1 promotes stress-induced RNA granule interactions to preserve polyadenylated mRNA. *J. Cell Biol.* **209**, 73–84 (2015).
18. Protter, D. S. W. & Parker, R. Principles and Properties of Stress Granules. *Trends Cell Biol.* **26**, 668–679 (2016).
19. Roth, T. L. *et al.* Reprogramming human T cell function and specificity with non-

viral genome targeting. *Nature* **559**, 405–409 (2018).

20. Ohashi, P. S. *et al.* Reconstitution of an active surface T3/T-cell antigen receptor by DNA transfer. *Nature* **316**, 606–609 (1985).
21. Koning, F., Lew, A. M., Maloy, W. L., Valas, R. & Coligan, J. E. The biosynthesis and assembly of T cell receptor alpha- and beta-chains with the CD3 complex. *J. Immunol.* **140**, 3126–3134 (1988).
22. Cochran, J. R., Aivazian, D., Cameron, T. O. & Stern, L. J. Receptor clustering and transmembrane signaling in T cells. *Trends Biochem. Sci.* **26**, 304–310 (2001).
23. Voon, D. C. *et al.* Use of mRNA- and protein-destabilizing elements to develop a highly responsive reporter system. *Nucleic Acids Res.* **33**, e27 (2005).
24. Hall, M. P. *et al.* Engineered luciferase reporter from a deep sea shrimp utilizing a novel imidazopyrazinone substrate. *ACS Chem. Biol.* **7**, 1848–1857 (2012).
25. Kalos, M. *et al.* T cells with chimeric antigen receptors have potent antitumor effects and can establish memory in patients with advanced leukemia. *Sci. Transl. Med.* **3**, 95ra73 (2011).
26. Kochenderfer, J. N. *et al.* Donor-derived CD19-targeted T cells cause regression of malignancy persisting after allogeneic hematopoietic stem cell transplantation. *Blood* **122**, 4129–4139 (2013).
27. Park, J. H. *et al.* Long-Term Follow-up of CD19 CAR Therapy in Acute Lymphoblastic Leukemia. *N. Engl. J. Med.* **378**, 449–459 (2018).
28. Eyquem, J. *et al.* Targeting a CAR to the TRAC locus with CRISPR/Cas9 enhances tumour rejection. *Nature* **543**, 113–117 (2017).
29. Courtney, A. H., Lo, W.-L. & Weiss, A. TCR Signaling: Mechanisms of Initiation and

Propagation. *Trends Biochem. Sci.* **43**, 108–123 (2018).

30. Au-Yeung, B. B. *et al.* A sharp T-cell antigen receptor signaling threshold for T-cell proliferation. *Proc. Natl. Acad. Sci. U. S. A.* **111**, E3679–88 (2014).
31. Au-Yeung, B. B. *et al.* IL-2 Modulates the TCR Signaling Threshold for CD8 but Not CD4 T Cell Proliferation on a Single-Cell Level. *J. Immunol.* **198**, 2445–2456 (2017).
32. Allison, K. A. *et al.* Affinity and dose of TCR engagement yield proportional enhancer and gene activity in CD4+ T cells. *Elife* **5**, (2016).
33. Richard, A. C. *et al.* T cell cytolytic capacity is independent of initial stimulation strength. *Nat. Immunol.* **19**, 849–858 (2018).
34. Iezzi, G., Karjalainen, K. & Lanzavecchia, A. The duration of antigenic stimulation determines the fate of naive and effector T cells. *Immunity* **8**, 89–95 (1998).
35. van Stipdonk, M. J., Lemmens, E. E. & Schoenberger, S. P. Naïve CTLs require a single brief period of antigenic stimulation for clonal expansion and differentiation. *Nat. Immunol.* **2**, 423–429 (2001).
36. Schrum, A. G., Palmer, E. & Turka, L. A. Distinct temporal programming of naive CD4+ T cells for cell division versus TCR-dependent death susceptibility by antigen-presenting macrophages. *Eur. J. Immunol.* **35**, 449–459 (2005).
37. Harding, F. A., McArthur, J. G., Gross, J. A., Raulet, D. H. & Allison, J. P. CD28-mediated signalling co-stimulates murine T cells and prevents induction of anergy in T-cell clones. *Nature* **356**, 607–609 (1992).
38. Harding, F. A. & Allison, J. P. CD28-B7 interactions allow the induction of CD8+ cytotoxic T lymphocytes in the absence of exogenous help. *J. Exp. Med.* **177**,

1791–1796 (1993).

39. Michel, F., Attal-Bonnefoy, G., Mangino, G., Mise-Omata, S. & Acuto, O. CD28 as a molecular amplifier extending TCR ligation and signaling capabilities. *Immunity* **15**, 935–945 (2001).
40. Green, J. M., Karpitskiy, V., Kimzey, S. L. & Shaw, A. S. Coordinate regulation of T cell activation by CD2 and CD28. *J. Immunol.* **164**, 3591–3595 (2000).
41. Green, J. M. *et al.* Absence of B7-dependent responses in CD28-deficient mice. *Immunity* **1**, 501–508 (1994).
42. Tuosto, L. & Acuto, O. CD28 affects the earliest signaling events generated by TCR engagement. *Eur. J. Immunol.* **28**, 2131–2142 (1998).
43. Shahinian, A. *et al.* Differential T cell costimulatory requirements in CD28-deficient mice. *Science* **261**, 609–612 (1993).
44. Kamphorst, A. O. *et al.* Rescue of exhausted CD8 T cells by PD-1-targeted therapies is CD28-dependent. *Science* **355**, 1423–1427 (2017).
45. Hui, E. *et al.* T cell costimulatory receptor CD28 is a primary target for PD-1-mediated inhibition. *Science* **355**, 1428–1433 (2017).
46. Jiang, Y., Chen, M., Nie, H. & Yuan, Y. PD-1 and PD-L1 in cancer immunotherapy: clinical implications and future considerations. *Hum. Vaccin. Immunother.* **15**, 1111–1122 (2019).
47. Watanabe, K., Kuramitsu, S., Posey, A. D., Jr & June, C. H. Expanding the Therapeutic Window for CAR T Cell Therapy in Solid Tumors: The Knowns and Unknowns of CAR T Cell Biology. *Front. Immunol.* **9**, 2486 (2018).
48. Mohammad, M. P., Munzarová Pondelícková, V., Zeman, J., Gunišová, S. &

Valášek, L. S. In vivo evidence that eIF3 stays bound to ribosomes elongating and terminating on short upstream ORFs to promote reinitiation. *Nucleic Acids Res.* **45**, 2658–2674 (2017).

49. Lin, Y. *et al.* eIF3 associates with 80S ribosomes to promote translation elongation, mitochondrial homeostasis, and muscle health. *bioRxiv* 651240 (2019) doi:10.1101/651240.
50. Bohlen, J., Fenzl, K., Kramer, G., Bukau, B. & Teleman, A. A. Selective 40S footprinting reveals that scanning ribosomes remain cap-tethered in human cells. *bioRxiv* 806364 (2019) doi:10.1101/806364.
51. Tan, H. *et al.* Integrative Proteomics and Phosphoproteomics Profiling Reveals Dynamic Signaling Networks and Bioenergetics Pathways Underlying T Cell Activation. *Immunity* **46**, 488–503 (2017).
52. Myers, D. R., Wheeler, B. & Roose, J. P. mTOR and other effector kinase signals that impact T cell function and activity. *Immunol. Rev.* **291**, 134–153 (2019).
53. Manfrini, N. *et al.* High levels of eukaryotic Initiation Factor 6 (eIF6) are required for immune system homeostasis and for steering the glycolytic flux of TCR-stimulated CD4+ T cells in both mice and humans. *Dev. Comp. Immunol.* **77**, 69–76 (2017).
54. Corcoran, D. L. *et al.* PARalyzer: definition of RNA binding sites from PAR-CLIP short-read sequence data. *Genome Biol.* **12**, R79 (2011).
55. Uko, N. E., Güner, O. F., Matesic, D. F. & Bowen, J. P. Akt Pathway Inhibitors. *Curr. Top. Med. Chem.* (2020) doi:10.2174/1568026620666200224101808.
56. Danan, C., Manickavel, S. & Hafner, M. PAR-CLIP: A Method for Transcriptome-Wide Identification of RNA Binding Protein Interaction Sites. *Methods Mol. Biol.*

1358, 153–173 (2016).

57. Bray, N. L., Pimentel, H., Melsted, P. & Pachter, L. Near-optimal probabilistic RNA-seq quantification. *Nat. Biotechnol.* **34**, 525–527 (2016).
58. Cunningham, F. *et al.* Ensembl 2019. *Nucleic Acids Res.* **47**, D745–D751 (2019).
59. Szklarczyk, D. *et al.* STRING v11: protein-protein association networks with increased coverage, supporting functional discovery in genome-wide experimental datasets. *Nucleic Acids Res.* **47**, D607–D613 (2019).
60. Wickham, H., Chang, W. & Others. ggplot2: Create elegant data visualisations using the grammar of graphics. *R package version* **2**, (2016).
61. Martin, M. Cutadapt removes adapter sequences from high-throughput sequencing reads. *EMBnet.journal* **17**, 10–12 (2011).
62. Frankish, A. *et al.* GENCODE reference annotation for the human and mouse genomes. *Nucleic Acids Res.* **47**, D766–D773 (2019).
63. Love, M. I., Huber, W. & Anders, S. Moderated estimation of fold change and dispersion for RNA-seq data with DESeq2. *Genome Biol.* **15**, 550 (2014).
64. Soneson, C., Love, M. I. & Robinson, M. D. Differential analyses for RNA-seq: transcript-level estimates improve gene-level inferences. *F1000Res.* **4**, 1521 (2015).
65. Zhu, A., Ibrahim, J. G. & Love, M. I. Heavy-tailed prior distributions for sequence count data: removing the noise and preserving large differences. *Bioinformatics* **35**, 2084–2092 (2019).
66. Schumann, K. *et al.* Generation of knock-in primary human T cells using Cas9 ribonucleoproteins. *Proc. Natl. Acad. Sci. U. S. A.* **112**, 10437–10442 (2015).

67. Parslow, A., Cardona, A. & Bryson-Richardson, R. J. Sample drift correction following 4D confocal time-lapse imaging. *J. Vis. Exp.* (2014) doi:10.3791/51086.

68. Noguchi, S. *et al.* FANTOM5 CAGE profiles of human and mouse samples. *Sci Data* **4**, 170112 (2017).

Extended Data Figures

Extended Data Figure 1. Composition of eIF3 in the Jurkat PAR-CLIP experiments. **a**, Composition of eIF3 in I+PMA activated and non-activated Jurkat cells after anti-EIF3B immunoprecipitation (IP), identified by mass spectrometry. Shown is an SDS polyacrylamide gel stained with Coomassie Brilliant Blue. **b**, Composition of eIF3 in activated Jurkat cells determined by western blot after anti-EIF3B IP. IN: input; FT: flow-through from anti-EIF3B IP beads; ELU: elution of eIF3 from anti-EIF3B IP beads. Anti-EIF4G1 and anti-RPS19 western blots confirm stringency of bead wash steps[5].

Extended Data Figure 2. Categories of RNA crosslinked to eIF3 by PAR-CLIP in Jurkat cells. PAR-CLIP crosslinking sites to eIF3, defined by clusters, divided into RNA categories, in I+PMA activated Jurkat cells (left) and non-activated Jurkat cells (right). In all panels, RNA categories include: 5'-UTR, 5'-UTR of mRNA; 3'-UTR, 3'-UTR of mRNA; CDS, protein coding region of mRNA; Start codon, beginning of mRNA CDS; Stop codon, stop codon region of mRNA; Intron, regions of pre-mRNA; Other, other classes of RNA; No annotation, reads that map to the human genome but that have no annotation assigned. Clusters in different mRNA categories may occur in the same mRNA species.

Extended Data Figure 3. Properties of PAR-CLIP sequence reads. a, The length distribution of PAR-CLIP clusters mapped to RNAs crosslinked to eIF3 in the EIF3A/C/B samples, from activated (left) and non-activated (right) Jurkat cells. **b**, The frequency

distribution of eIF3 PAR-CLIP clusters mapped to RNAs in the EIF3A/C/B samples, from activated (left) and non-activated (right) Jurkat cells. In all panels, the distributions are the average of both biological replicates. RNA PAR-CLIP properties observed in the EIF3A/C/B sample are representative of those seen in PAR-CLIP sequence reads of RNAs crosslinked to other eIF3 subunits.

Extended Data Figure 4. Comparison of transcription profiles and PAR-CLIP reads. MA plots of **a**, non-activated Jurkat cells compared to Jurkat cells activated with I+PMA for 5 hours (left) and HEK293T cells compared to Jurkat cells activated with I+PMA for 5 hours (right). In **a**, M = $\log_2$(HEK293T mRNA TPM/Jurkat mRNA TPM), and A = mean(TPM) for activated Jurkat mRNAs. TPM, transcripts per million. The FDR was set to 0.01, and the blue dots indicate significant fold changes. **b,** Scatterplot of TPM of mRNAs expressed in activated Jurkat cells (most abundant isoform, see Methods) versus mRNAs identified by PAR-CLIP as crosslinked to eIF3, with ≥ 100 total read counts.

Extended Data Figure 5. eIF3-mRNA crosslinking patterns in activated Jurkat cells. a, mRNAs sorted by increasing value of the ratio of normalized 5'-UTR reads to normalized 3'-UTR reads. Values of the ratio of 5'-UTR/3'-UTR normalized reads > 200 have been truncated to a value of 200 in the plot (asterisk). The arrow indicates the threshold used to create cumulative plots shown in **Figure 2a**. **b**, Examples of eIF3 crosslinking to histone mRNAs *HIST1H2AI* and *HIST1H3H* are shown. Transcription start sites were determined from the FANTOM5 Database[68].

Extended Data Figure 6. *TCRA* and *TCRB* mRNA localization patterns. a, Single plane image of TetraSpeck microspheres (100 nm) adjacent to Jurkat cell probed for P bodies (far left). Scatter plots of pixel intensities in different emission channels are shown: channel 1, 670 nm; channel 2, 570 nm; channel 3, 488 nm. Plots left to right are: channel 1 vs. channel 2, channel 1 vs. channel 3, and channel 2 vs. channel 3. **b**, Single plane image of Jurkat cell probed for *TCRA* mRNA (channel 1), *TCRB* mRNA (channel 2), and DCP1 to mark P bodies (channel 3). Scatter plots to the right are shown as in **a**. **c**, Single plane image and scatter plots for TetraSpeck microspheres as in **a**, but adjacent to Jurkat cell probed for stress granules. **d**, Single plane image of Jurkat cell probed for *TCRA* mRNA (channel 1), *TCRB* mRNA (channel 2), and G3BP1 to mark stress granules (channel 3). Scatter plots to the right are shown as in **a**.

Extended Data Figure 7. CRISPR/Cas9 RNP mediated genome editing at the *TCRA* and *TCRB* genomic loci in primary human T cells. a, Location of gRNA sites targeting the *TCRA* 3'-UTR, to generate *TCRA* Δ*PAR* cells. In *TCRA*, gRNA1 and gRNA2 target hg38 genomic locations chr14:22,551,700 and chr14:22,552,073, respectively. **b**, PCR primers flanking the *TCRA* editing sites. **c**, Analysis of *TCRA* 3'-UTR PAR-CLIP site deletion efficiency. Total genomic DNA extracted from WT, *TCRA* Δ*PAR, TCRB* Δ*PAR* (here serving as a negative control), scrambled gRNA nucleofected (S) and non-nucleofected (N) cells was analyzed by PCR to measure the editing efficiency. *TCRA* Δ*PAR* cells produced a 1283 bp PCR product compared to 1676 bp in S, N or *TCRB* Δ*PAR* cells. **d**, Location of gRNA sites of targeting the *TCRB*

3'-UTR, to generate *TCRB* Δ*PAR* cells. In *TCRB*, gRNA1 and gRNA2 target hg38 genomic locations chr7:142,802,561 and chr7:142,802,695. **e**, PCR primers flanking the *TCRB* editing sites. **f**, Analysis of *TCRB* 3'-UTR PAR-CLIP site deletion efficiency. Total genomic DNA extracted from WT, *TCRA* Δ*PAR* (here serving as a negative control), *TCRB* Δ*PAR*, scrambled gRNA nucleofected (S) and non-nucleofected (N) cells were analyzed by PCR to measure the editing efficiency. *TCRB* Δ*PAR* cells produced a 1022 bp PCR product compared to 1190 bp in S, N or *TCRA* Δ*PAR* cells.

Extended Data Figure 8. TCR levels on the cell surface of primary human T cells. **a**, Percentage of cells expressing TCR on the cell surface measured by flow cytometric analysis (*n = 2* donors). TCR expressing cells in the cell populations tested: *1gB*, *TCRB* gRNA 1; *2gB*, *TCRB* gRNA 2; *1+2 gB*, *TCRB* gRNA 1+2 (i.e. *TCRB* Δ*PAR*); *1gA*, *TCRA* gRNA 1; *2gA*, *TCRA* gRNA 2; *1+2 gA*, *TCRA* gRNA 1+2 (i.e. *TCRA* Δ*PAR*); Δ*TCR*, TCR gRNA targeting the CDS of *TCRA*; *N*, Non-nucleofected cells; SC, Scrambled gRNA. (*n* = 2 donors, with standard deviation shown.) Left: I+PMA activated T cells, after 3 hours of activation; Right: non-activated T cells. P values for *TCRA* Δ*PAR*, *TCRB* Δ*PAR,* Δ*TCR* were < 0.0001 relative to SC in both activated and non-activated cells, using one-way ANOVA. The P values for single guide edited non-activated cells relative to SC were not significant, while in activated cells P = 0.02 – 0.05 relative to SC. **b,** Representative density plots showing the percentage of TCR on the cell surface in non activated T cells for one of the two donors. The cell lines shown are: *TCRA* Δ*PAR*, *TCRB* Δ*PAR*, Δ*TCR* (negative control), and SC.

Extended Data Figure 9. Gating strategy for flow cytometric analysis of CD69 and CD25 levels. Primary human T cells were gated to isolate lymphocytes, followed by isolation of single cells, then live cells. Next, cells were gated to separate CD4+ and CD8+ cells expressing T cell activation markers CD69 and CD25 after activation with anti-CD3/anti-CD28 antibodies. Shown is the workflow of the FACS gating, with an example of T cells activated with anti-CD3/anti-CD28 antibodies for 8 hours.

Extended Data Figure 10. Phenotypic analysis of CD8+ primary human T cells with eIF3 3'-UTR PAR-CLIP sites deleted. Flow cytometric analysis of CD8+ T cells, showing quantification of T cell activation markers CD69 (early activation marker) and CD25 (mid-activation marker) after activation with anti-CD3/anti-CD28 antibodies at different time points, for all cell populations tested: *1gB*, *TCRB* gRNA 1; *2gB*, *TCRB* gRNA 2; *1+2 gB*, *TCRB* gRNA 1+2 (i.e. *TCRB* Δ*PAR*); *1gA*, *TCRA* gRNA 1; *2gA*, *TCRA* gRNA 2; *1+2 gA*, *TCRA* gRNA 1+2 (i.e. *TCRA* Δ*PAR*); *ΔTCR* gRNA targeting the CDS of *TCRA*; N, Non-nucleofected cells; SC, Scrambled gRNA. ($n = 2$ donors, with mean and standard deviation shown). P values for *TCRA* Δ*PAR*, *TCRB* Δ*PAR,* Δ*TCR* were < 0.0001 relative to SC, while single gRNA edited cell lines had $P < 0.0001$ to $P < 0.01$, relative to SC as calculated by two-way ANOVA.

Extended Data Figure 11. Phenotypic analysis of CD4+ primary human T cells with eIF3 3'-UTR PAR-CLIP sites deleted. a, Flow cytometric analysis of CD4+ T cells, showing quantification of T cell activation markers CD69 (early activation marker) and CD25 (mid-activation marker) after activation with anti-CD3/anti-CD28 antibodies at

different time points, for all cell populations tested: *1gB*, *TCRB* gRNA 1; *2gB*, *TCRB* gRNA 2; *1+2 gB*, *TCRB* gRNA 1+2 (i.e. *TCRB* Δ*PAR*); *1gA*, *TCRA* gRNA 1; *2gA*, *TCRA* gRNA 2; *1+2 gA*, *TCRA* gRNA 1+2 (i.e. *TCRA* Δ*PAR*); *ΔTCR* gRNA targeting the CDS of *TCRA*; N, Non-nucleofected cells; SC, Scrambled gRNA. (*n = 2* donors, with mean and standard deviation shown). P values for *TCRA* Δ*PAR*, *TCRB* Δ*PAR,* Δ*TCR* were < 0.0001 relative to SC, while single gRNA edited cell lines had P < 0.0001 to P < 0.01, relative to SC as calculated by two-way ANOVA. **b**, Representative density plots showing the percentage of cells expressing CD69, CD69 and CD25 or CD25 only, for one of two donors. The cell lines shown are *TCRA* Δ*PAR*, *TCRB* Δ*PAR*, Δ*TCR* (negative control), and SC.

Extended Data Figure 12. Cytokine secretion profile of primary human T cells with with eIF3 3'-UTR PAR-CLIP sites deleted. Quantification of **a**, secreted IL2 and **b,** secreted IFNγ, for all cell populations tested, as determined by ELISA. Cell populations tested were: *1gB*, *TCRB* gRNA 1; *2gB*, *TCRB* gRNA 2; *1+2 gB*, *TCRB* gRNA 1+2 (i.e. *TCRB* Δ*PAR*); *1gA*, *TCRA* gRNA 1; *2gA*, *TCRA* gRNA 2; *1+2 gA*, *TCRA* gRNA 1+2 (i.e. *TCRA* Δ*PAR*); *ΔTCR* gRNA targeting the CDS of *TCRA*; N, Non-nucleofected cells; SC, Scrambled gRNA. (*n = 2* donors, with mean and standard deviation shown.) P values for *TCRA* Δ*PAR*, *TCRB* Δ*PAR,* Δ*TCR* were < 0.0001 relative to SC, while single gRNA edited cell lines had P < 0.0001 to P < 0.01, relative to SC as calculated by two-way ANOVA.

Extended Data Figure 13. TCR protein and RNA levels in Jurkat cells with eIF3 3'-UTR PAR-CLIP sites deleted. a, Western blots measuring TCRA protein levels as a function of time after anti-CD3/anti-CD28 activation. Cell lines are indicated by transcript structure above the western blots. HSP90 was used as a loading control. **b**, *TCRA* and *TCRB* mRNA levels in WT Jurkat cells, or Jurkat cells with the *TCRA* eIF3 3'-UTR PAR-CLIP site deleted, as determined by qRT-PCR at different time points after anti-CD3/anti-CD28 activation. **c**, *TCRA* and *TCRB* mRNA levels in WT Jurkat cells, or Jurkat cells with the *TCRB* eIF3 3'-UTR PAR-CLIP site deleted, as determined by qRT-PCR at different time points after anti-CD3/anti-CD28 activation. (*n* = *2*, with mean ± standard deviations shown), **** P < 0.0001, *** P < 0.001, ** P < 0.01 for *TCRA* Δ*PAR* or *TCRB* Δ*PAR* relative to WT, using two-way ANOVA.

Extended Data Figure 14. TCR mRNA binding to eIF3 in Jurkat cells. Immunoprecipitation of eIF3 using an anti-EIF3B antibody[5] , followed by qRT-PCR to quantify the amount of **a**, *TCRA* or **b**, *TCRB* mRNA bound to eIF3. Jurkat cells with or without the eIF3 PAR-CLIP site in the 3'-UTR were analyzed after activation with anti-CD3/anti-CD28 antibodies for 5 hours (left) and 8 hours (right). Percent mRNA bound to anti-EIF3B beads relative to total mRNA isolated from the cells (*TCRA* or *TCRB* on the left, *IL2* on the right). (*n* = 3, with mean and standard deviations shown). For *TCRA* and *TCRB* mRNAs, P < 0.0001 relative to WT. P values for IL2 mRNAs for Δ*PAR* relative to WT were not significant using two-way ANOVA. The schematic of the experiment is shown in **Figure 5c**.

Extended Data Figure 15. TCR clustering in Jurkat cells. WT, *TCRA* Δ*PAR, TCRB* Δ*PAR* cells exhibiting TCR clustering, as determined using anti-TCRA/anti-TCRB protein staining and Airyscan confocal microscopy. Cells were activated with anti-CD3/anti-CD28 antibodies for 5 hours (left) and 8 hours (right). (*n = 5* for each time point after activation for all cell lines, with representative images shown)

Extended Data Figure 16. Phenotypic analysis of Jurkat cells. a, Flow cytometric analysis of cells expressing T cell activation markers CD69 (early activation marker) and CD25 (mid-activation marker) in WT, *TCRA* Δ*PAR* or *TCRB* Δ*PAR* Jurkat cells at different time points after stimulation with anti-CD3/anti-CD28 antibodies. (*n* = 3, with mean and standard deviations shown). Left graph, $P < 0.0001$ for CD69 expression in *TCRA* Δ*PAR* and *TCRB* Δ*PAR* cells relative to WT cells using one-way ANOVA. Right graph, $P < 0.001$ for CD69 and CD25 expression of *TCRA* Δ*PAR* and *TCRB* Δ*PAR* relative to WT using two-way ANOVA. **b**, Density plots showing cell populations expressing CD69+ only, CD69+ CD25+ or CD25+ only from WT, *TCRA* Δ*PAR* or *TCRB* Δ*PAR* Jurkat cells at different time points after stimulation with anti-CD3/anti-CD28 antibodies, (*n = 3*, with representative plots shown). (**c**) Quantification of secreted IL2 from WT, *TCRA* Δ*PAR* or *TCRB* Δ*PAR* cells at different time points after stimulation with anti-CD3/anti-CD28 antibodies, as determined by ELISA. (*n* = 3, with mean and standard deviation shown.) $P < 0.0001$ for *TCRA* Δ*PAR* and *TCRB* Δ*PAR* cells relative to WT cells, as determined by two-way ANOVA.

Extended Data Figure 17. Effect of *TCRA*, *TCRB* 3'-UTRs and 3'-UTR variants measured by nanoluciferase reporters. a, Changes in nanoluciferase mRNA levels in the experiment shown in **Fig. 5b**, as determined by qRT-PCR. $P < 0.0001$ for *TCRA* Δ*PAR* relative to WT at 8 hr, and for *TCRA* Δ*PAR* and R**PAR* relative to WT at 10 hr, using two-way ANOVA. $P \leq 0.0002$ for *TCRB* Δ*PAR*and R**PAR* relative to WT at 8 hr and 10 hr. **b,** the absolute luciferase levels in anti-CD3/anti-CD28 antibody activated Jurkat cells stably expressing the nanoluciferase reporter normalized with the 1 hr time point shown in **Fig. 5d**. (*n* = 3, with mean and standard deviations shown). The stably expressed nanoluciferase reporters in Jurkat cells have either the intact 3'-UTR from *TCRA* (left axis), the Woodchuck Hepatitis Virus (WHP) Posttranscriptional Regulatory Element (*WPRE*, right axis), the gammaretroviral 3'-Long terminal repeat (*3'-LTR*, right axis), or the bovine growth hormone polyadenylation signal (*bpA*, right axis) following the nanoluciferase coding sequence as shown in the schematic in **Fig. 5d**. $P < 0.0001$ for all the time points when comparing *WPRE*, *3'-LTR*, or *bpA* with the *TCRA* 3'-UTR, using two-way ANOVA.

Extended Data Figure 18. Regulatory pathways leading to dynamics of TCR protein expression levels. a, Western blots of TCRA protein levels in Jurkat cells using different activation modes. **b,** Western blot of TCRA protein levels in Jurkat cells activated with anti-CD3/anti-CD28 antibodies in the presence of AKT inhibitors MK2206 and GSK690693. An anti-Phospho-GSK-3β antibody was used to measure AKT activity, and experiments with AKT inhibitors were carried out in duplicate. In all panels HSP90 was used as a loading control.

Supplementary Information

Supplementary Figures 1-3: Raw images of gels used for Fig. 1b, Fig. 3a, Extended Data Fig. 1, and Extended Data Fig. 13a.

Supplementary Table 1: Subunits in eIF3 crosslinked to RNA in activated Jurkat cells. Lists the eIF3 subunits, percent sequence coverage and number of identified peptides.

Supplementary Table 2: PARpipe statistics for eIF3 PAR-CLIP samples. Samples are indexed in the first tab, including both biological replicates for activated and non-activated Jurkat cells. Statistics are given for each library at the read, cluster and group level.

Supplementary Table 3: PAR-CLIP mapping to individual genes for each eIF3 PAR-CLIP sample. Samples are indexed in the first tab, including both biological replicates for activated and non-activated Jurkat cells. First lists the gene name and number of clusters identified. The statistics also include: Sum, sum of that statistic over all sites for that gene; Med, median of that statistic for all sites for that gene; ReadCount, total reads mapping to the gene; T2Cfraction, number of reads with T-to-C conversions / number of reads; ConversionSpecificity, log(number of reads with T-to-C conversions / number of reads with other conversions); UniqueReads, reads collapsed to single copies. Also included: 5'utr/Intron/Exon/3'utr/Start_codon/Stop_codon, number of sites mapping to that annotation category; Junction, number of sites mapping to a junction between

categories (coding-intron, coding-3'utr, etc.); GeneType, as described in the gene_type category for this gene in the .gtf file used.

Supplementary Table 4. Transcriptome analysis of HEK293T cells and non-activated or activated Jurkat cells. Each tab lists transcript name and version, gene name, type of transcript, length of transcript, and mean transcripts per million, calculated from two biological replicates.

Supplementary Table 5. Differential expression analysis of HEK293T or non-activated vs. activated Jurkat cells. Each tab lists the gene name, mean of normalized counts, $\log_2$-fold change, $\log_2$-fold change standard error, Wald statistic, Wald test P-value, and Benjamini-Hochberg adjusted P-value.

Supplementary Table 6. Pathway enrichment analysis. Lists for both biological replicates of the EIF3A/C/B PAR-CLIP libraries are included (genes with >= 100 reads), along with associated transcript names, lengths in nts of the 5'-UTR, coding region, and 3'-UTR, and reads normalized to the lengths of the transcript regions. Tabs also include the top tissue-specific pathway enrichment categories determined using the STRING Database. These list: the Gene Ontology (GO) number, GO description, observed gene count, background gene count, false discovery rate, and matching proteins in the network by Ensembl protein ID, and by gene name.

Supplementary Table 7. Reagent information for experiments. Lists include antibodies used, PCR primers, qPCR primers, gRNA targeting sequences, FISH probes, and 3'-UTR sequences.

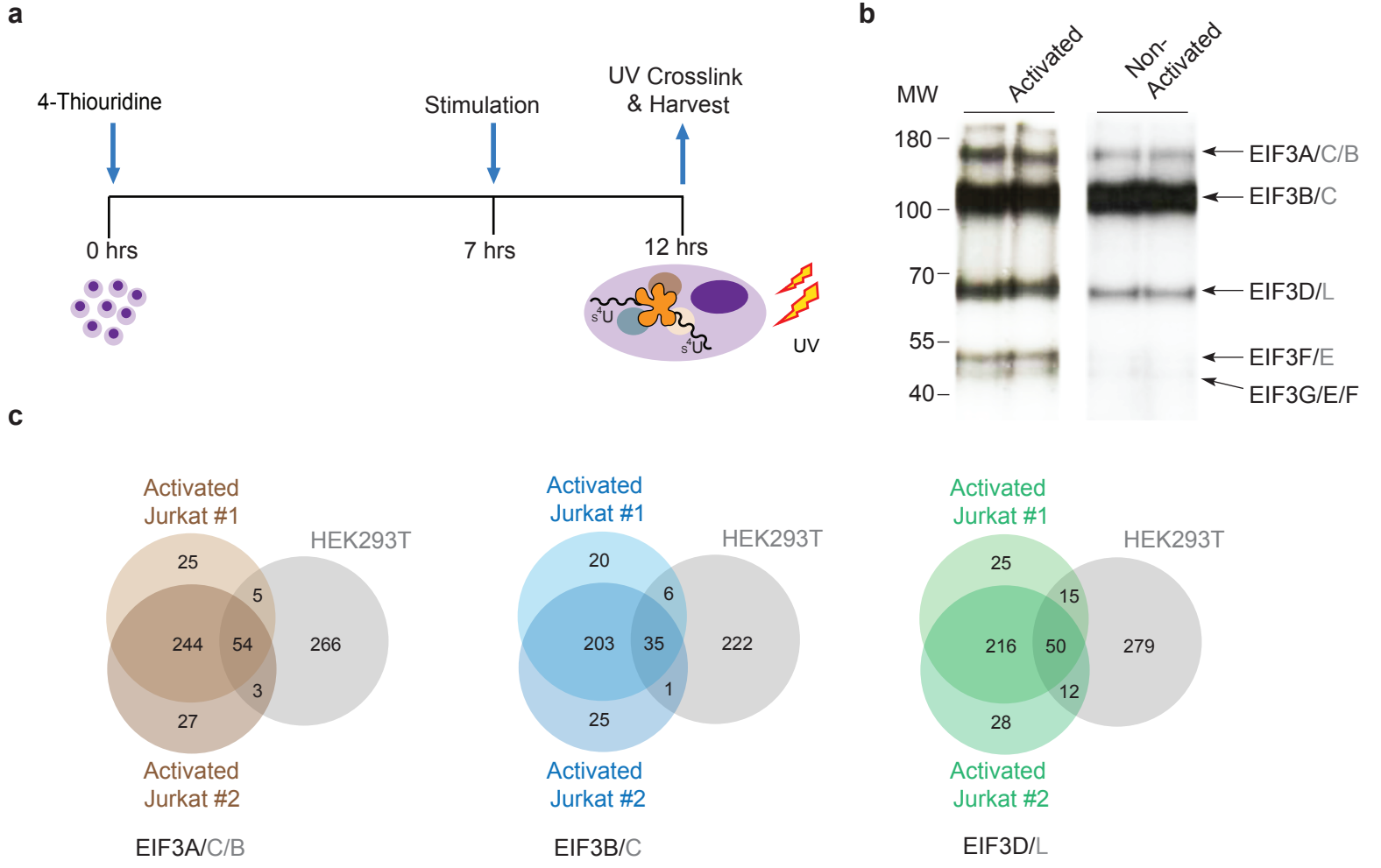
a
4-Thiouridine
Stimulation
UV Crosslink
& Harvest
0 hrs
7 hrs
12 hrs
UV
b
MW
Activated
Non-Activated
180
100
70
55
40
EIF3A/C/B
EIF3B/C
EIF3D/L
EIF3F/E
EIF3G/E/F
c
Activated Jurkat #1
HEK293T
Activated Jurkat #2
25
5
244
54
266
3
27
EIF3A/C/B
Activated Jurkat #1
HEK293T
Activated Jurkat #2
20
6
203
35
222
1
25
EIF3B/C
Activated Jurkat #1
HEK293T
Activated Jurkat #2
25
15
216
50
279
12
28
EIF3D/L

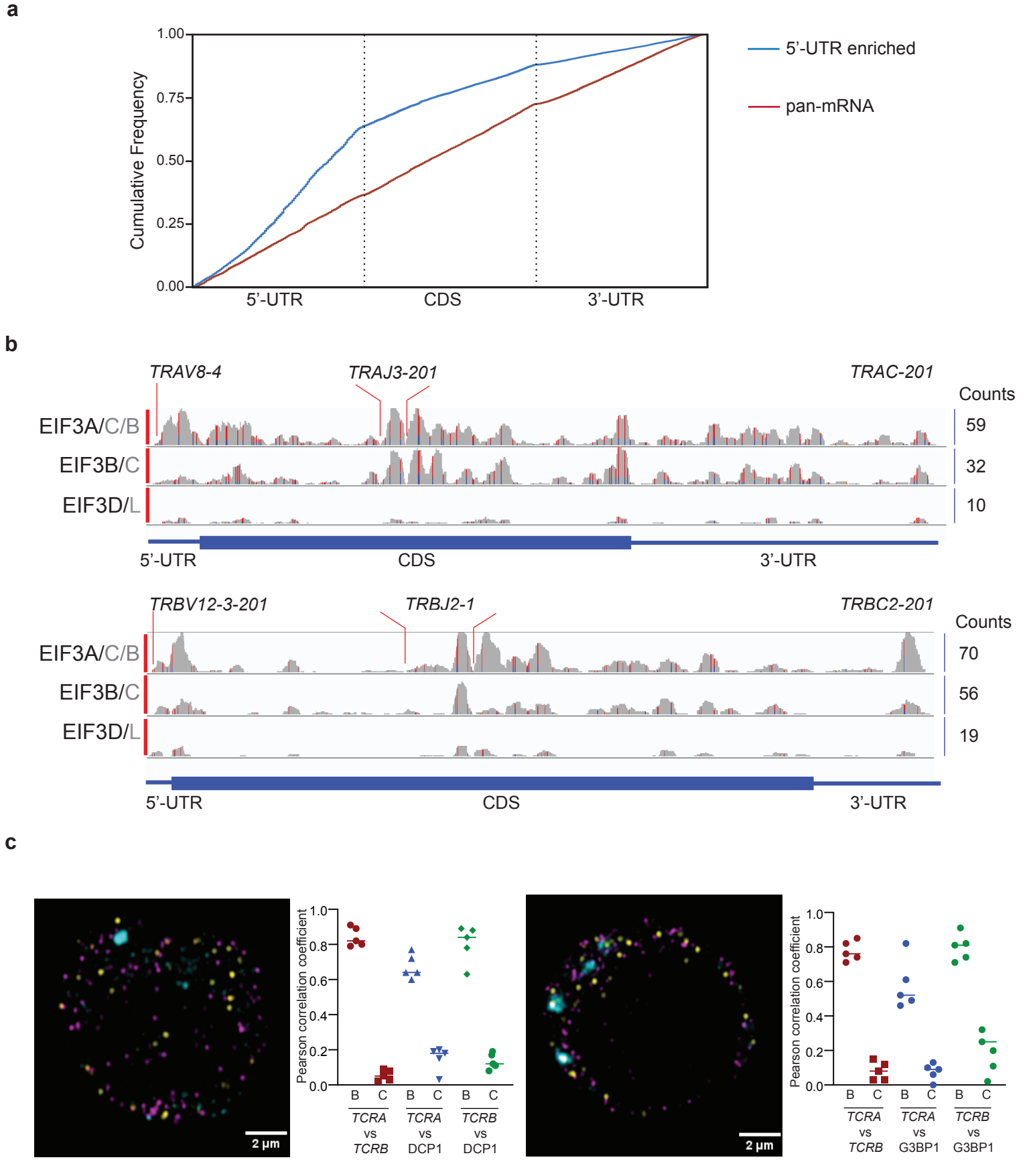
a
Cumulative Frequency
1.00
0.75
0.50
0.25
0.00
5'-UTR
CDS
3'-UTR
5'-UTR enriched
pan-mRNA
b
TRAV8-4
TRAJ3-201
TRAC-201
Counts
EIF3A/C/B
EIF3B/C
EIF3D/L
59
32
10
5'-UTR
CDS
3'-UTR
TRBV12-3-201
TRBJ2-1
TRBC2-201
Counts
EIF3A/C/B
EIF3B/C
EIF3D/L
70
56
19
5'-UTR
CDS
3'-UTR
c
2 µm
Pearson correlation coefficient
1.0
0.8
0.6
0.4
0.2
0.0
B C B C B C
TCRA vs TCRB
TCRA vs DCP1
TCRB vs DCP1
2 µm
Pearson correlation coefficient
1.0
0.8
0.6
0.4
0.2
0.0
B C B C B C
TCRA vs TCRB
TCRA vs G3BP1
TCRB vs G3BP1

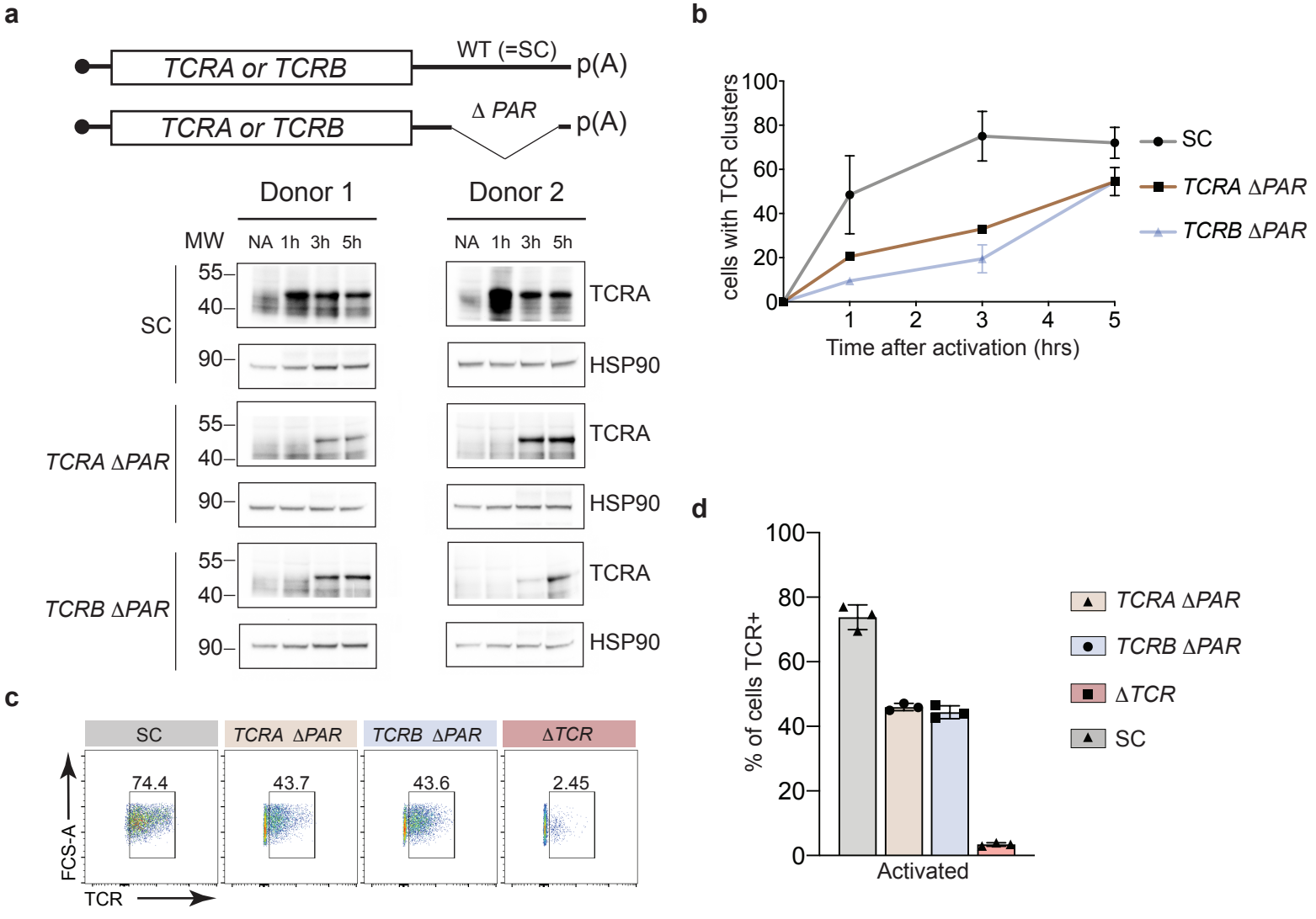
a
TCRA or TCRB
WT (=SC)
p(A)
TCRA or TCRB
Δ PAR
p(A)
Donor 1
Donor 2
MW
NA 1h 3h 5h
NA 1h 3h 5h
55
40
90
SC
TCRA ΔPAR
TCRB ΔPAR
TCRA
HSP90
b
cells with TCR clusters
Time after activation (hrs)
SC
TCRA ΔPAR
TCRB ΔPAR
c
SC
TCRA ΔPAR
TCRB ΔPAR
ΔTCR
74.4
43.7
43.6
2.45
FCS-A
TCR
d
% of cells TCR+
Activated
TCRA ΔPAR
TCRB ΔPAR
ΔTCR
SC

a

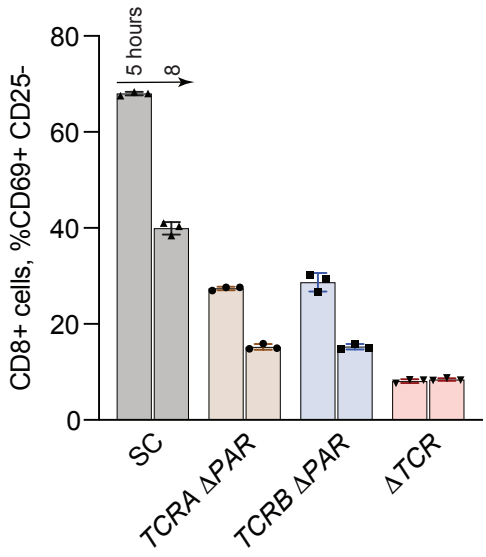
CD8+ cells, %CD69+ CD25-
5 hours
8
80
60
40
20
0
SC
TCRA ΔPAR
TCRB ΔPAR
ΔTCR

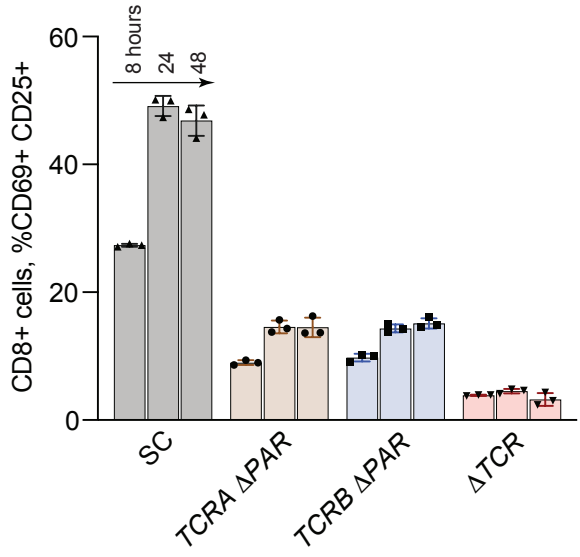
CD8+ cells, %CD69+ CD25+
8 hours
24
48
60
40
20
0
SC
TCRA ΔPAR
TCRB ΔPAR
ΔTCR

b

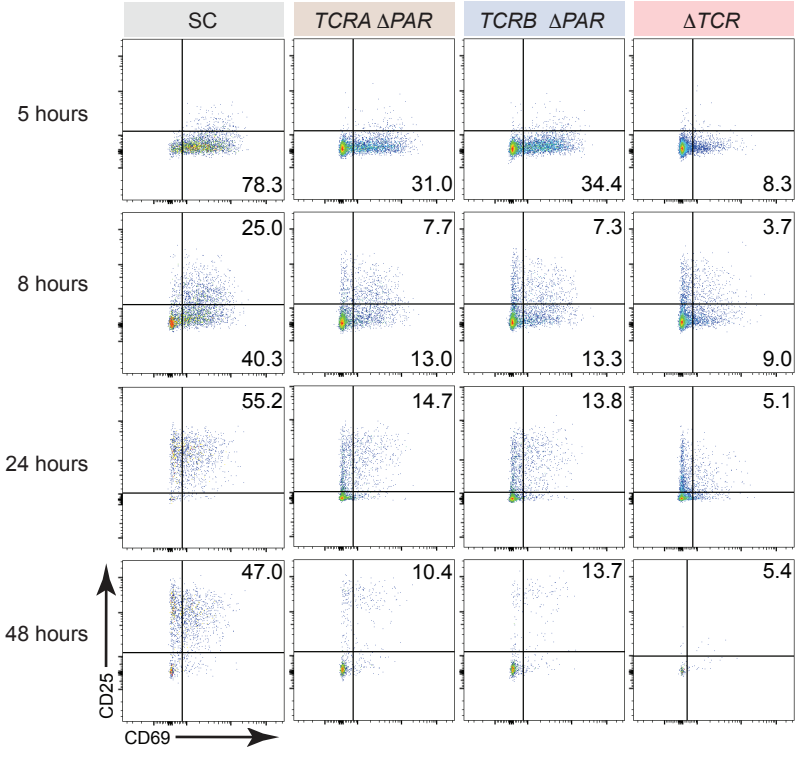
SC
TCRA ΔPAR
TCRB ΔPAR
ΔTCR
5 hours
8 hours
24 hours
48 hours
78.3
31.0
34.4
8.3
25.0
7.7
7.3
3.7
40.3
13.0
13.3
9.0
55.2
14.7
13.8
5.1
47.0
10.4
13.7
5.4
CD25
CD69

c

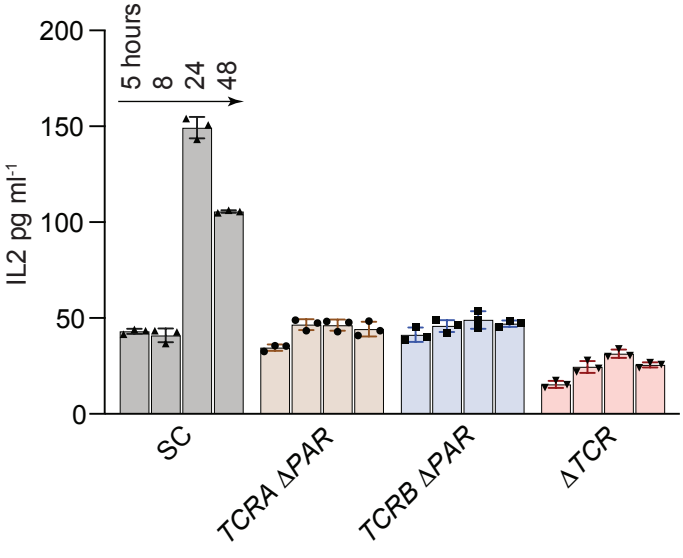
IL2 pg ml-1
5 hours
8
24
48
200
150
100
50
0
SC
TCRA ΔPAR
TCRB ΔPAR
ΔTCR

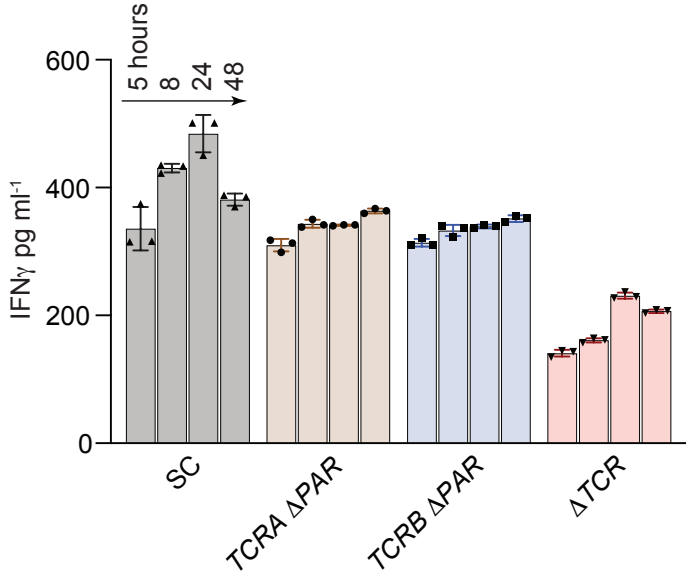
IFNγ pg ml-1
5 hours
8
24
48
600
400
200
0
SC
TCRA ΔPAR
TCRB ΔPAR
ΔTCR

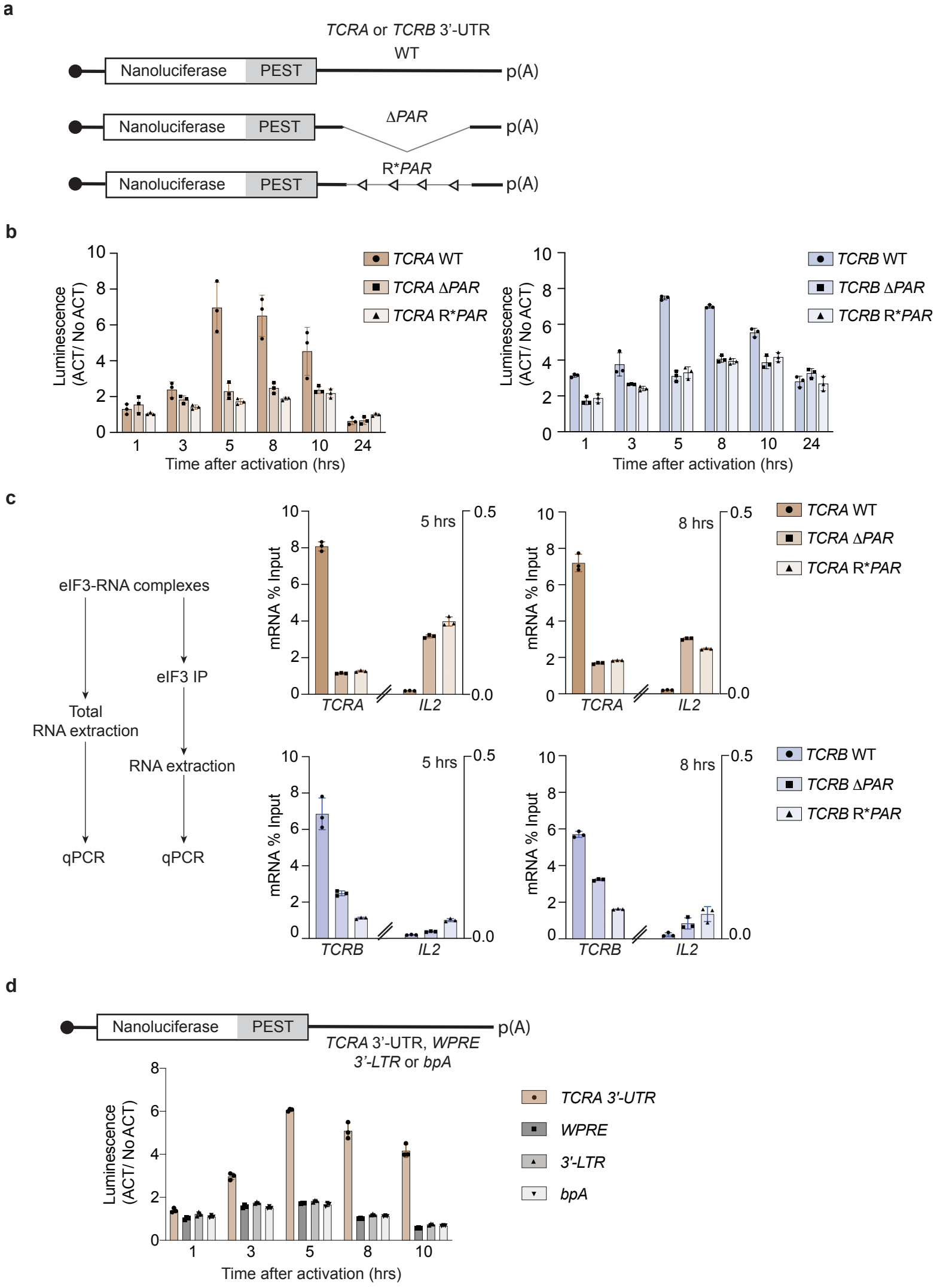
a
TCRA or TCRB 3'-UTR
WT
Nanoluciferase
PEST
p(A)
ΔPAR
R*PAR
b
Luminescence (ACT/ No ACT)
Time after activation (hrs)
TCRA WT
TCRA ΔPAR
TCRA R*PAR
TCRB WT
TCRB ΔPAR
TCRB R*PAR
c
eIF3-RNA complexes
eIF3 IP
Total RNA extraction
RNA extraction
qPCR
mRNA % Input
5 hrs
8 hrs
TCRA
IL2
TCRB
d
TCRA 3'-UTR, WPRE 3'-LTR or bpA
TCRA 3'-UTR
WPRE
3'-LTR
bpA

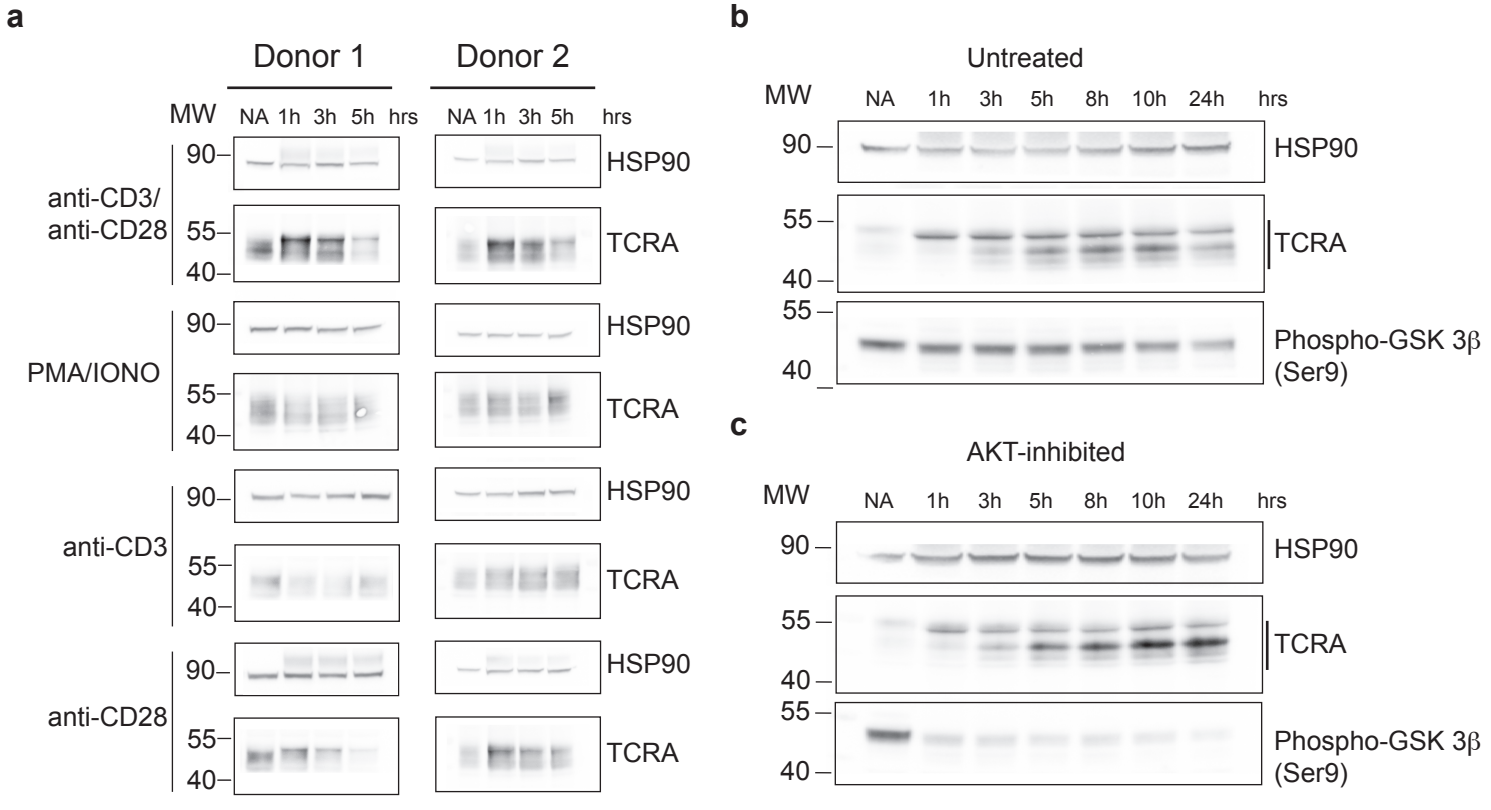
a
Donor 1
Donor 2
MW
NA 1h 3h 5h hrs
NA 1h 3h 5h hrs
anti-CD3/
anti-CD28
PMA/IONO
anti-CD3
anti-CD28
90
55
40
HSP90
TCRA
b
Untreated
MW
NA 1h 3h 5h 8h 10h 24h hrs
90
55
40
55
40
HSP90
TCRA
Phospho-GSK 3β
(Ser9)
c
AKT-inhibited
MW
NA 1h 3h 5h 8h 10h 24h hrs
90
55
40
55
40
HSP90
TCRA
Phospho-GSK 3β
(Ser9)